



Determining the quantitative relationship between glycolysis and GAPDH in cancer cells exhibiting the Warburg effect

Received for publication, January 14, 2021, and in revised form, January 29, 2021 Published, Papers in Press, February 3, 2021,
<https://doi.org/10.1016/j.jbc.2021.100369>

Xiaobing Zhu[‡], Chengmeng Jin[‡], Qiangrong Pan, and Xun Hu*

From the Cancer Institute (Key Laboratory for Cancer Intervention and Prevention, China National Ministry of Education, Zhejiang Provincial Key Laboratory of Molecular Biology in Medical Sciences), The Second Affiliated Hospital, Zhejiang University School of Medicine, Hangzhou, China

Edited by John Denu

Previous studies have identified GAPDH as a promising target for treating cancer and modulating immunity because its inhibition reduces glycolysis in cells (cancer cells and immune cells) with the Warburg effect, a modified form of cellular metabolism found in cancer cells. However, the quantitative relationship between GAPDH and the aerobic glycolysis remains unknown. Here, using siRNA-mediated knockdown of GAPDH expression and iodoacetate-dependent inhibition of enzyme activity, we examined the quantitative relationship between GAPDH activity and glycolysis rate. We found that glycolytic rates were unaffected by the reduction of GAPDH activity down to $19\% \pm 4.8\%$ relative to untreated controls. However, further reduction of GAPDH activity below this level caused proportional reductions in the glycolysis rate. GAPDH knockdown or inhibition also simultaneously increased the concentration of glyceraldehyde 3-phosphate (GA3P, the substrate of GAPDH). This increased GA3P concentration countered the effect of GAPDH knockdown or inhibition and stabilized the glycolysis rate by promoting GAPDH activity. Mechanistically, the intracellular GA3P concentration is controlled by the Gibbs free energy of the reactions upstream of GAPDH. The thermodynamic state of the reactions along the glycolysis pathway was only affected when GAPDH activity was reduced below $19\% \pm 4.8\%$. Doing so moved the reactions catalyzed by GAPDH + PGK1 (phosphoglycerate kinase 1, the enzyme immediate downstream of GAPDH) away from the near-equilibrium state, revealing an important biochemical basis to interpret the rate control of glycolysis by GAPDH. Collectively, we resolved the numerical relationship between GAPDH and glycolysis in cancer cells with the Warburg effect and interpreted the underlying mechanism.

Aerobic glycolysis (Warburg effect [WE]) is a prominent feature of cancer cells. The WE is crucial for the growth, survival, metastasis, and drug resistance of cancer cells (1–4). Regulating glycolysis *via* targeting the rate-limiting enzymes in glycolysis has been recognized as a promising approach to treat cancer (5–8). Classically, HK2, PFK1, and pyruvate kinase (PK) are the rate-

limiting enzymes, as they catalyze irreversible reactions under physiological conditions and they are sensitive to allosteric regulations (9–13). The remaining glycolytic enzymes are generally not considered as rate-limiting enzymes, as the reactions that they catalyze are reversible under physiological conditions.

A recent study (14) based on metabolic control analysis and computer simulations in several models of simplified metabolic pathways questions the long-standing hypothesis that reactions far from thermodynamic equilibriums, such as the reactions catalyzed by hexokinase (HK), PFK1, and PK, are the rate-limiting steps in a pathway. Instead, the regulation of metabolic flux in a pathway that contains reactions near equilibrium depends more on distribution of the Gibbs free energy among reaction steps in the pathway than on the Gibbs free energy of the reaction catalyzed by the given enzyme.

GAPDH attracted much attention recently (6–8, 15–19) and was recognized as a potential therapeutic target because of its reported role in the rate control of glycolysis in cells with the Warburg phenotype, such as cancer cells and activated myeloid and lymphoid cells. Although the findings are promising for cancer treatment or immunity modulation, the detailed quantitative relationship between GAPDH and glycolysis has not been demonstrated. If a candidate drug interrupts glycolysis primarily *via* inhibiting GAPDH, it is essential that the numerical relationship between GAPDH and glycolysis be established, as this is the fundamental logic. We sought to investigate the quantitative relationship between GAPDH and aerobic glycolysis to delineate the biochemical insight into this relationship.

Results

Cell lines

We used five cancer cells lines for this work, cervical cancer cell line HeLa, gastric cancer cell line MGC80-3, colon cancer cell line RKO, liver cancer cell line SK-HEP-1, and lung cancer cell line A549. These cell lines exhibited the WE, as described by us recently (20).

GAPDH specific activity, the concentration of GAPDH, and GAPDH actual activity

In this study, the GAPDH specific activity (GAPDH-SA) refers to the activity assayed at the saturating substrate

[‡] These authors contributed equally to this work.

* For correspondence: Xun Hu, huxun@zju.edu.cn.

Glycolysis and GAPDH in cancer cells

concentration. The concentration of the GAPDH is derived from the equation $V_{\text{specific-activity}} \approx V_{\text{max}} = k_{\text{cat}}[E]$: we set the relative concentration of GAPDH in the control cells as 100%, then the relative concentration of GAPDH in the cells treated with siRNA or GAPDH inhibitor would be the following.

$$[\text{GAPDH}]_{\text{treated}} = \frac{\text{GAPDH-SA}_{\text{treated}}}{\text{GAPDH-SA}_{\text{ctrl}}} [\text{GAPDH}]_{\text{ctrl}} \quad (1)$$

The GAPDH actual activity (GAPDH-AA) refers to its activity at the actual concentration of its substrates in the glycolysis.

The quantitative relationship between the glycolysis rate and GAPDH—siRNA knockdown model

siGAPDH specifically knocked down GAPDH-SA with no or marginal effect on the activities of other glycolytic enzymes (Fig. 1). The knockdown efficiency ranged from 48% (RKO) to 72% (HeLa) (Fig. 2, A and B). GAPDH knockdown marginally affected glucose (Glc) consumption and lactate generation (Fig. 2C) in HeLa, RKO, MGC80-3, and SK-HEP-1 cells. In A549 cells, GAPDH knockdown moderately reduced lactate production by about 15% but with a marginal reduced Glc consumption, in comparison with the control (Fig. 2C). The data suggested that the effect of GAPDH knockdown may vary from cell to cell, but the variation was moderate.

Although GAPDH-knockdown cells produced a lactate amount comparable with control cells, it could be that a fraction of lactate produced by GAPDH-knockdown cells was from other metabolic pathways, so that the total lactate amount was not less than that in control cells. To exclude this possibility, we used [$^{13}\text{C}_6$]glucose to trace lactate in cells and demonstrated that about 95% lactate ($m + 3$) generated by control and GAPDH knockdown cells was from Glc (Fig. S1).

However, siRNA knockdown could not generate serial clones with a stepwise decrement of GAPDH activity, so that the quantitative relationship between GAPDH and aerobic glycolysis could not be established.

The quantitative relationship between glycolysis rate and GAPDH—GAPDH titration in living cells by IA

Iodoacetate (IA) is a GAPDH inhibitor (21–23), as well as a thiolate reagent. We did a serial of quality controls.

We measured the activities of glycolytic enzymes in the cell lysate prepared from HeLa, RKO, MGC80-3, SK-HEP-1, and A549, which were pretreated with IA (Fig. 3A). It is noted that even when GAPDH-SA was inhibited by 98.5%, the activities of other glycolytic enzymes were not significantly different from untreated controls.

Cells were incubated in a serial of concentrations of IA (1–100 μM) for 7 h. The cellular GSH content did not change significantly at the IA concentration between 0 and 10 μM (Fig. 3B). At 25 μM IA, there was a moderate reduction of the cellular GSH concentration (by 23% and 15% for HeLa and RKO, respectively) but no statistical significance. When the IA concentration increased to 50 μM , the cellular GSH concentration was significantly reduced. The result was consistent with the previous report (24). In contrast, when cells were treated with IA at the concentration range between 0 and 25 μM , the GAPDH activity was inversely proportional to the IA concentration (Fig. 3C). GAPDH activity was significantly inhibited even by 1 μM IA. When IA was 25 μM , the residual activity of GAPDH only retained 2.6% and 1.1% for HeLa and RKO, respectively. Moreover, IA at the effective concentration inactivating GAPDH did not significantly affect other glycolytic enzymes (Fig. 3A).

We prepared cell lysate from HeLa and RKO and measured the inhibition of GAPDH-SA by IA. The inhibition curve was similar between HeLa and RKO (Fig. 3D). Therefore, the inhibition is cell-type independent.

We measured the stability of GAPDH-SA in the cell lysate prepared from HeLa and RKO pretreated with IA (Fig. 3E). The data showed that GAPDH-SA was stable. This stable inhibition is important for real-time monitor of the GAPDH-SA in the subsequent study, otherwise the quantitative relationship between GAPDH and the aerobic glycolysis in cells could not be established.

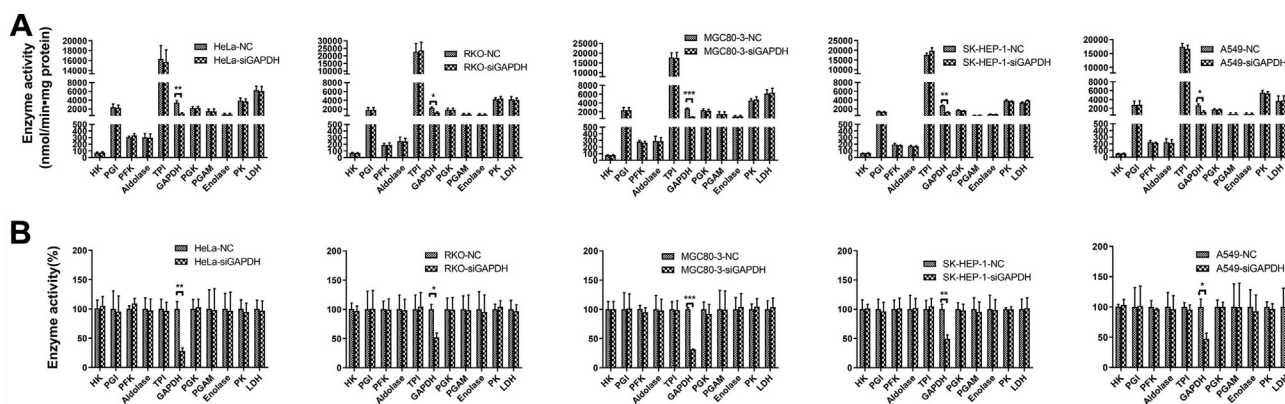


Figure 1. siGAPDH specifically reduced the GAPDH activity without significantly affecting other glycolytic enzymes. A, specific activity. B, relative activity. Cells were transfected with siGAPDH or control siRNA for 48 h, and cells were collected for analysis of enzyme activity as described in [Experimental procedures](#). Data are from [Table S1](#). * $p < 0.05$, ** $p < 0.01$, and *** $p < 0.001$ by two-tailed Student's t test. Data are the mean \pm SEM from three independent experiment.

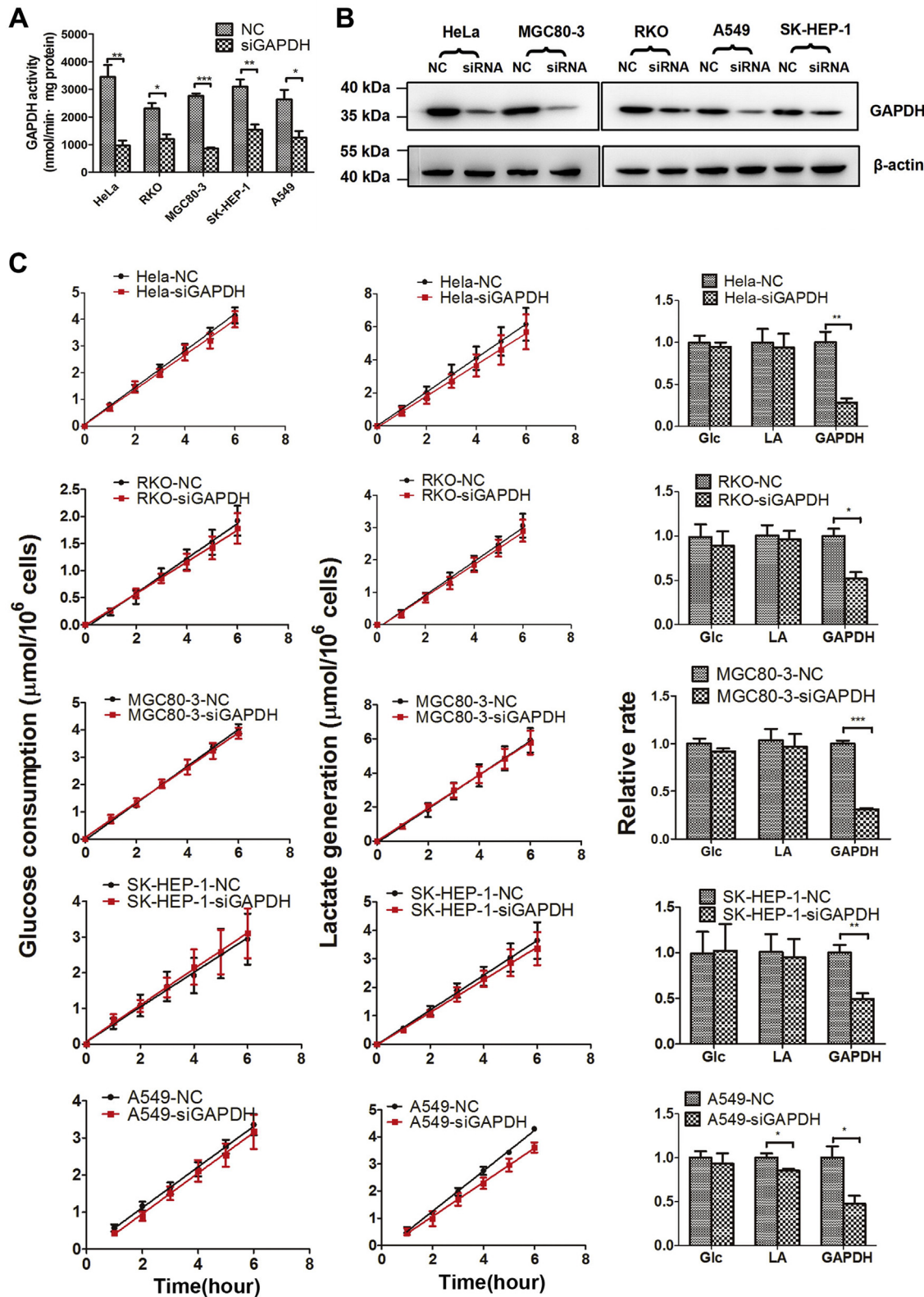


Figure 2. Knockdown of GAPDH marginally perturbed glycolysis. A, GAPDH activity and (B) Western blot of GAPDH in cells with or without GAPDH knockdown. C, the glucose consumption rate and lactate generation rate in cells with or without GAPDH knockdown (left and middle panels); the right panels compare the relative rates of glucose consumption, lactate generation, and GAPDH, showing that the reduction of GAPDH is virtually irrelevant with the rates of glucose consumption and lactate generation; the relative glucose consumption rate and relative lactate generation rate are based on the data in the left and middle panels. Data are from Table S1. * $p < 0.05$, ** $p < 0.01$, and *** $p < 0.001$ by two-tailed Student's t test. Data are the mean \pm SEM from three independent experiments.

Glycolysis and GAPDH in cancer cells

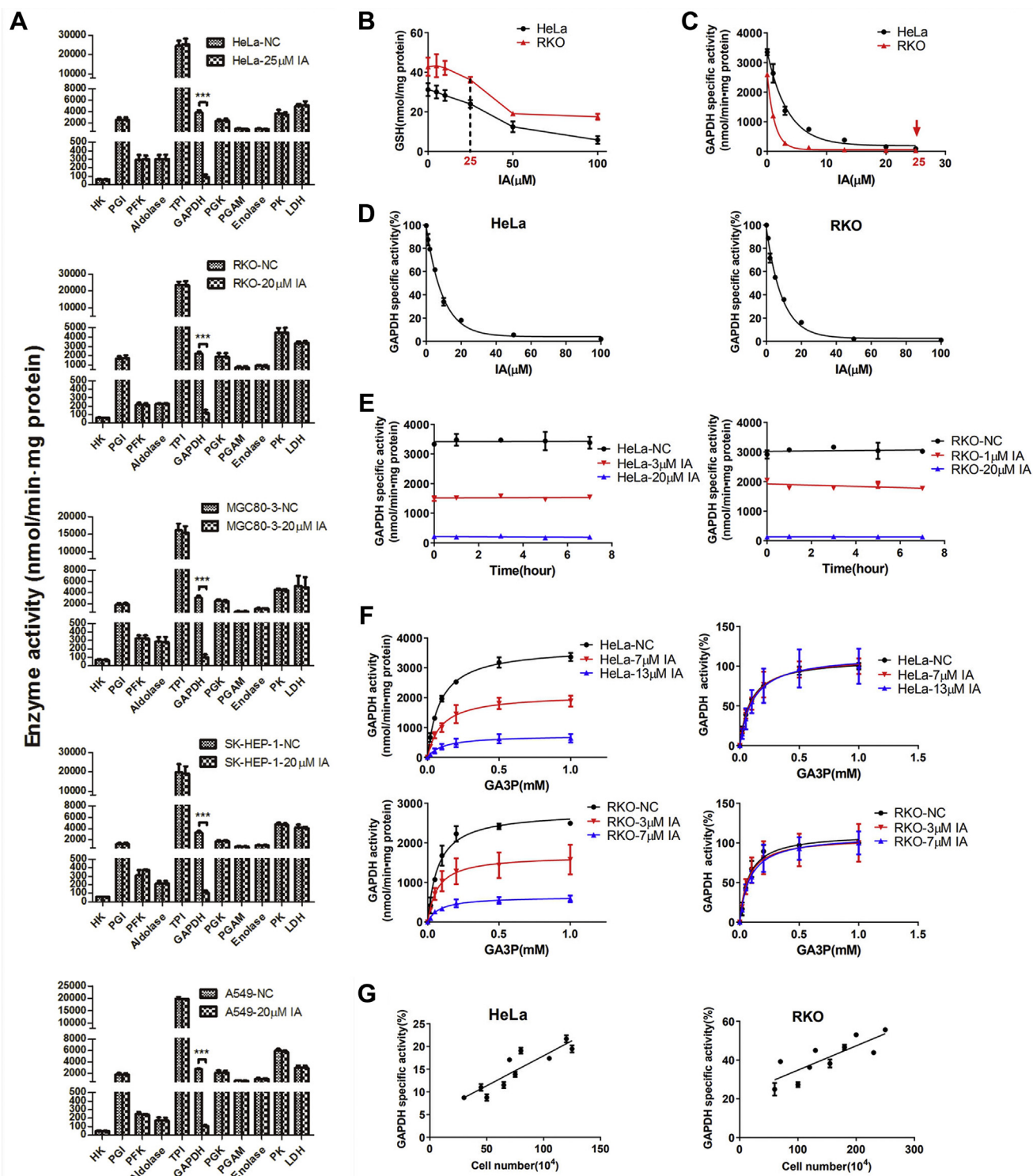


Figure 3. Quality controls for IA inhibition of GAPDH. A, IA specifically inhibits GAPDH without significantly affecting other glycolytic enzymes. Cells were treated with IA with the indicated concentration for 6 h, and cells were collected and lysed. Enzyme activities in the cell lysate were measured as described in [Experimental procedures](#). Data are from [Table S2](#). B and C, the different effect of IA on cellular GSH and GAPDH. Cells were treated with IA at the indicated concentrations for 7 h and then collected and subjected for GSH quantification or GAPDH activity. D, GAPDH activity versus IA concentration. HeLa or RKO cell lysate (HeLa, 3.6 mg protein/ml; RKO, 4.8 mg protein/ml) was mixed with IA at the indicated concentrations at 4 °C for 30 min and followed by GAPDH activity determination. E, the inhibition stability of GAPDH by IA. HeLa or RKO cells were pretreated with IA at indicated concentrations for 2 h. Cells were collected and lysed. The GAPDH activity in the cell lysate was monitored at the indicated intervals for 7 h. F, Left panel, GAPDH activity versus [GA3P], right panel, GAPDH activity% versus [GA3P]. HeLa or RKO cells were pretreated with IA at the indicated concentrations for 2 h. Cells were collected and lysed. GAPDH rate versus [GA3P] was carried out. G, the relationship between the cell density and inhibition efficiency of GAPDH by IA. HeLa cells were treated with 7 μM for 5 h, and RKO cells were treated with 3 μM for 2 h. Cells were collected and lysed. GAPDH activity in the cell lysate was determined. *** $p < 0.001$ by two-tailed Student's *t* test. Data are the mean \pm SEM from three independent experiments. IA, iodoacetate.

We also did the substrate-dependent kinetics of GAPDH in the cell lysate from HeLa and RKO cells with or without IA treatment. When converting the kinetic rate to percentage, they were identical (Fig. 3F), indicating that IA inhibition only reduced the concentration of functional GAPDH without affecting the kinetic feature of the enzyme.

Finally, we checked if cell density would affect the inhibition efficacy of IA. The results showed that IA efficacy decreased with the increase in the cell number (Fig. 3G). Therefore, in the subsequent experiments, we fixed the seeding cell number.

We then treated HeLa cells with IA. At the indicated intervals, we collected cells and medium, measured GAPDH-SA (Fig. 4A), Glc consumption (Fig. 4B), and lactate generation (Fig. 4C). We then deduced the instantaneous rate of change of Glc consumption ($V_{i\text{-glucose}}$) (Fig. 4D) and lactate generation ($V_{i\text{-lactate}}$) (Fig. 4E) by differentiating the data of Figure 4, B and C and correlated the GAPDH-SA with $V_{i\text{-glucose}}$ (Fig. 4F) and $V_{i\text{-lactate}}$ (Fig. 4G).

The quantitative relationship between GAPDH-SA and $V_{i\text{-lactate}}$ appeared to be composed of two functions (Fig. 4G). When GAPDH-SA% was between $23.8\% \pm 3\%$ and 100% (Table 1), the $V_{i\text{-lactate}}$ was a constant, the function could be expressed by

$$f(x) = c \quad (2)$$

When GAPDH-SA% was below $23.8\% \pm 3\%$, $V_{i\text{-lactate}}$ was positively correlated with GAPDH-SA%, the relationship could be expressed by the following:

$$f(x) = ax / (b + x) \quad (3)$$

where x refers the GAPDH-SA%. The half maximal $V_{i\text{-lactate}}$ corresponded to $8.1\% \pm 0.7\%$ GAPDH-SA in HeLa cells (Table 1). The relationship between GAPDH-SA% and $V_{i\text{-glucose}}$ exhibited a similar pattern (Fig. 4F) to that between GAPDH-SA% and $V_{i\text{-lactate}}$.

Using the same approach, we obtained the curves between Glc consumption or lactate generation and the GAPDH-SA in RKO, SK-HEP-1, MGC80-3, and A549. (Figs. S2–S5). Again, the quantitative relationship between Glc consumption or lactate generation and the GAPDH-SA could be grouped into two functions, as described for HeLa cells. The half maximal

$V_{i\text{-lactate}}$ corresponded to $3.5\% \pm 0.4\%$ GAPDH-SA for RKO cells, $6.7\% \pm 0.4\%$ GAPDH-SA for MGC80-3 cells, $4.1\% \pm 0.6\%$ GAPDH-SA for SK-Hep-1 cells, and $4.8\% \pm 0.7\%$ GAPDH-SA for A549 cells (Table 1). The data revealed a high similarity of the quantitative relationship between the glycolysis and GAPDH in the five cancer cell lines.

We summarized the quantitative relationship between GAPDH-SA% and the glycolysis rate derived from the five cell lines in Table 1. The equations numerically correlate the glycolysis rate to GAPDH-SA% and introduce two critical values of the glycolysis rate that were achieved at two critical points of GAPDH-SA%. The first critical point of GAPDH-SA% is $19\% \pm 4.8\%$; above this point, the glycolysis rate is a constant, and below this point, the glycolysis rate decreased according to Equation 3. The second critical point of GAPDH-SA% is $5.4\% \pm 1.9\%$, at which the glycolysis rate is decreased by half. Numerically, the glycolysis rate *versus* GAPDH-SA% is equivalent to the glycolysis rate *versus* the concentration of GAPDH.

The quantitative relationship between GAPDH-SA, cell growth, growth inhibition, and cell death

We treated HeLa cells with serial concentrations of IA and monitored the cell growth, Glc consumption, lactate generation, and GAPDH-SA in a time course (Fig. 5, A–D). The data demonstrated an association between the variables (IA, GAPDH-SA, glycolysis, and cell growth). To better correlate the quantitative nature of these variables, we extracted the data of the 24 h point.

We first correlated IA with the glycolysis rate and cell growth (Fig. 5, E and F). The IC_{50} of IA for Glc consumption and lactate generation were 9.0 and 9.5 μM , respectively, which were close to the IC_{50} (8.2 μM) of IA for cell growth inhibition. The cell number were positively correlated with the glycolysis rate (Fig. 5, G and H).

Then, we correlated IA with GAPDH. The IC_{50} of IA for GAPDH-SA was 2.5 μM (Fig. 5I), which was much lower than the IC_{50} for glycolysis and cell growth.

By plotting GAPDH-SA with the glycolysis rate, the half inhibition of Glc consumption and lactate generation corresponded to 6.8% and 6.5% GAPDH-SA, respectively (Fig. 5, J and K), which were consistent to the data in Figure 4.

Table 1
The aerobic glycolysis (V) as a function of the GAPDH specific activity as a variable

	GAPDH-SA%					
	HeLa	RKO	MGC80-3	SK-HEP-1	A549	Combined ^a
$V = c = V_{\text{max}}^b$	100–23.8 \pm 3	100–15.3 \pm 1.8	100–18.7 \pm 1.6	100–13.5 \pm 3.4	100–23.9 \pm 2.3	100–19 \pm 4.8
$V = \frac{a(\text{GAPDH-SA}\%)}{b+(\text{GAPDH-SA}\%)}$	<23.8 \pm 3	<15.3 \pm 1.8	<18.7 \pm 1.6	<13.5 \pm 3.4	<23.9 \pm 2.3	<19 \pm 4.8
Critical GAPDH-SA% point that saturates the flux	23.8 \pm 3	15.3 \pm 1.8	18.7 \pm 1.6	13.5 \pm 3.4	23.9 \pm 2.3	19 \pm 4.8
Critical GAPDH-SA% point that corresponds to 1/2 V_{max}	8.1 \pm 0.7	3.5 \pm 0.4	6.7 \pm 0.4	4.1 \pm 0.6	4.8 \pm 0.7	5.4 \pm 1.9

GAPDH-SA, GAPDH specific activity.

^a The mean \pm SD of five cell lines. Data of HeLa, RKO, MGC80-3, SK-HEP-1, and A549 are the mean \pm SEM from three independent experiments.

^b The glycolytic rate (V) in the control cells whose GAPDH-SA is 100%.

Glycolysis and GAPDH in cancer cells

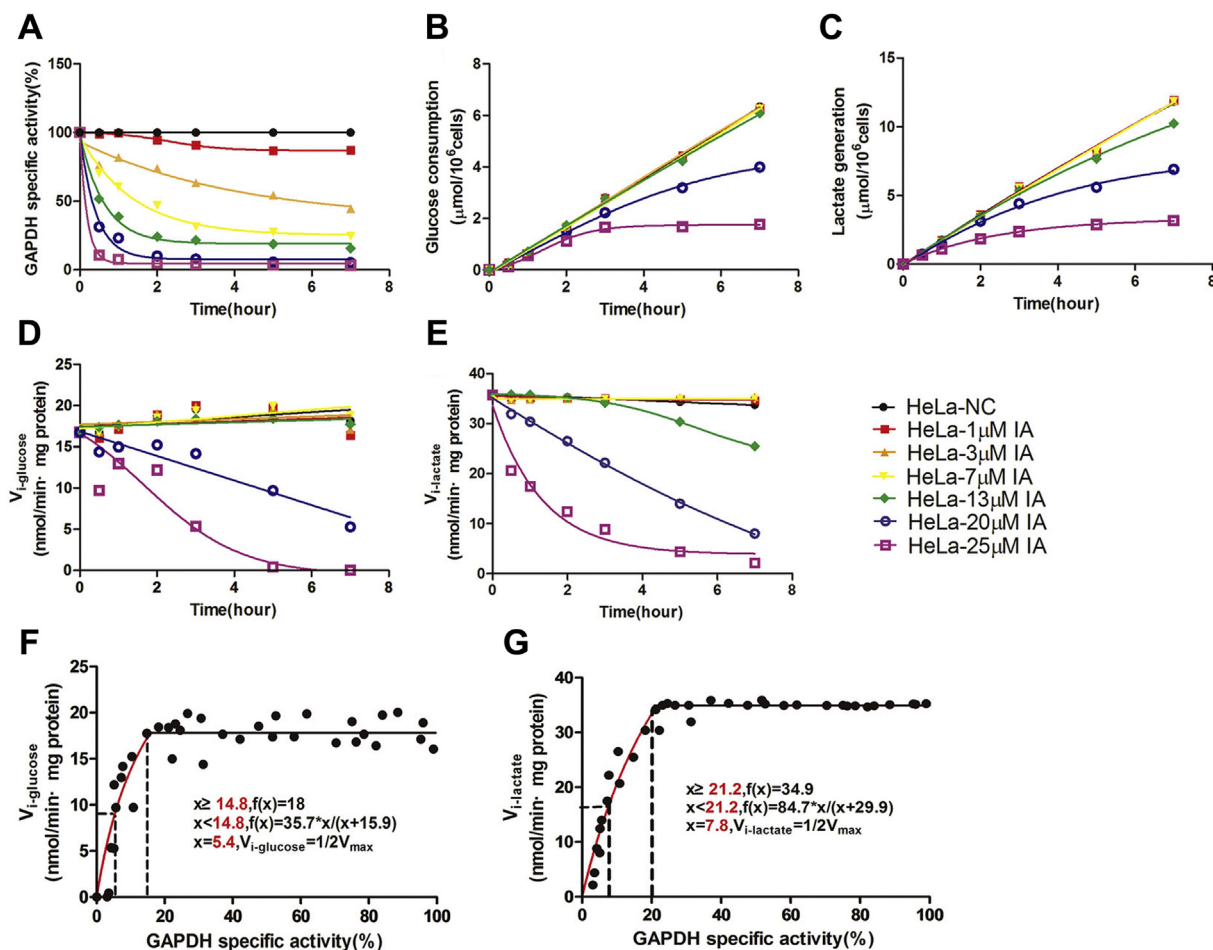


Figure 4. Correlating the aerobic glycolysis rate with GAPDH activity in HeLa cells. HeLa cells were treated with IA at the indicated concentrations for a time course of 7 h. At each interval in the time course, cells were collected and lysed, and GAPDH activity in the cell lysate was measured; medium glucose and lactate concentrations were measured. *A*, GAPDH activity in the cell lysate. *B*, consumption of glucose. *C*, generation of lactate. *D*, instantaneous rate of change of glucose consumption ($V_{i\text{-glucose}}$) by differentiating data in panel *B*. *E*, instantaneous rate of change of lactate generation ($V_{i\text{-lactate}}$) by differentiating data in panel *C*. *F*, $V_{i\text{-glucose}}$ versus GAPDH activity, $V_{i\text{-glucose}}$ from panel *D*, and GAPDH activity from panel *A*. x refers to GAPDH specific activity, $f(x)$ refers to the $(V_{i\text{-glucose}})$, the V_{max} is defined by the rate at the critical point, above which the rate is a constant. *G*, $V_{i\text{-lactate}}$ versus GAPDH activity, $V_{i\text{-lactate}}$ from panel *E*, and GAPDH activity from panel *A*. Data are the mean \pm SD from one representative experiment from three independent experiments. This is to show the process how we derive the equation. The data combined from three independent experiments are summarized in Table 1.

Cell growth *versus* GAPDH-SA conveyed the following information (Fig. 5L). We dissected the line into three segments. Cell growth was not affected by perturbing GAPDH-SA from 100% and 42.9% (the black segment); cell growth was inhibited by further reducing GAPDH-SA from 42.9% and 9.5% (green segment); and cell death occurred by further inhibiting GAPDH-SA% down to <9.5% (red segment).

We then used RKO to repeat the same experiments, and we obtained the similar results (Fig. S6).

We were curious about if the cells treated with 8 μM IA could resume proliferation. We treated HeLa and RKO cells with 8 μM IA for 48 h. The residual GAPDH-SA only retained 2.3% and 4.5% in HeLa and RKO, respectively, and cell growth was completely inhibited. We then removed the drug by displacing the medium. GAPDH activity recovered by 75% and 72%, respectively, in HeLa and RKO cells at the 72 h point after displacing the medium. Cells partially resumed proliferation (Fig. S7).

The quantitative relationship between GAPDH-SA and its substrate GA3P

It is noted that when GAPDH-SA% in cells varied from 100% to 19% \pm 4.8%, the lactate generation rate kept constant. As the lactate generation rate kept constant, the rate through GAPDH in the glycolysis must also keep constant. Then why GAPDH-SA reduced from 100% to 19% does not affect the rate through GAPDH in the glycolysis?

We found that GAPDH knockdown was associated with an increase of [GA3P] in cells, consistent in five cell lines (Fig. 6A). In IA titration experiments, [GA3P] was incrementally increased, accompanied with a corresponding decrement of GAPDH-SA (Fig. 6B). The reciprocal relationship between [GAPDH] and [GA3P] could be expressed quantitatively by Equation 4 (Fig. 6C):

$$f(x) = C / (Ax + B) \quad (4)$$

where $f(x)$ and x refer [GA3P] and GAPDH-SA%, respectively.

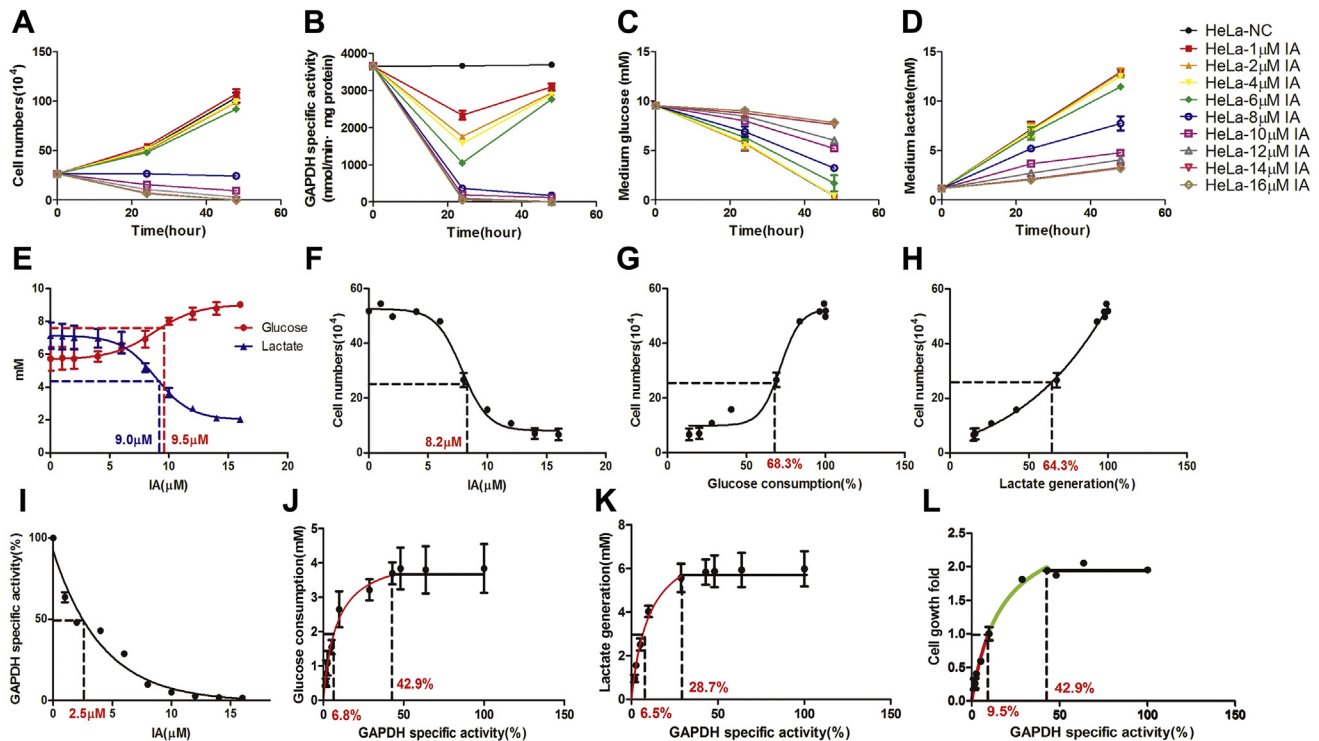


Figure 5. Correlating glycolysis or cell status with IA or GAPDH-SA. A–D, HeLa cells were treated with IA at the indicated concentrations. At indicated time points, cell numbers were counted, GAPDH-SA in the cell lysate was measured, medium glucose and lactate concentrations were measured. The data of the 24 h point were used for further correlation in panels E to L. E, correlating glucose consumption and lactate generation with IA. The point that the red dotted line crosses at the red solid line corresponds to the IC₅₀ of IA for glucose consumption, and the point that the blue dotted line crosses at the blue solid line corresponds to the IC₅₀ of IA for lactate generation. F, correlating cell growth with IA. The point that the dotted line crosses at the solid line corresponds to the IC₅₀ of IA for cell growth. G and H, correlating cell growth with glucose consumption and lactate generation. The point that dotted lines cross at the solid line corresponds to the 1/2 cell growth of the control. I, correlating GAPDH activity with IA. J and K, note the critical point that corresponds to GAPDH-SA 42.9% and 28.7%, which separates the quantitative relationship between glycolysis and GAPDH into two functions, when GAPDH-SA is from 100% to 42.9% $V_{\text{glucose}} = C$, when GAPDH-SA is smaller than 42.9%, $V_{\text{glucose}} = ax/(b + x)$; when GAPDH-SA is from 100% to 28.7% $V_{\text{lactate}} = C$, when GAPDH-SA is smaller than 28.7%, $V_{\text{lactate}} = ax/(b + x)$, where x is GAPDH-SA%. The 1/2 glucose consumption and lactate generation correspond to GAPDH-SA at GAPDH-SA 6.8% and 6.5%, respectively. L, correlating cell growth with GAPDH-SA. The onefold indicates the cell number at the start point. The folds larger than 1 indicate cell growth, and the folds smaller than 1 indicate cell death. The line is empirically divided into three segments: cell growth is not affected in the black segment, cell growth was inhibited in the green segment, and negative cell growth (cell death) was in the red segment. Data are the mean \pm SEM from three independent experiments. GAPDH-SA, GAPDH specific activity; IA, iodoacetate.

The most fundamental principle of enzyme kinetics is that the catalytic rate of an enzyme is the function of the concentrations of both the enzyme and its substrate. The K_m values of GAPDH were 0.065 to 0.11 mM (Fig. S8), consistent with the reported value (25, 26). The cellular [GA3P] in untreated cells was 0.031 to 0.061 mM (Table S4), which were not saturating GAPDH. Therefore, the increased [GA3P] could increase GAPDH activity and countered the effect of GAPDH knockdown or inhibition. Based on the information, we propose that the rate through GAPDH in the glycolysis is balanced by the concentration of both GAPDH and glyceraldehyde 3-phosphate (GA3P), that is, the reciprocal relationship of the concentrations between GAPDH and GA3P could compensate each other and stabilize the rate through GAPDH in the glycolysis.

The next question is to what extent the increased GA3P concentration could compensate the decreased GAPDH activity induced by GAPDH knockdown or inhibition. This issue requires determination of the GAPDH-AA. However, as the GAPDH in cells is compartmented (27–29), we were not able to figure out the fraction of [GAPDH] in cells that is directly

participating in glycolysis, so that we could not estimate GAPDH-AA in cells.

The quantitative relationship between the glycolysis rate, GA3P, and GAPDH-AA in the cell-free glycolysis

To correlate GAPDH-AA with the glycolysis rate, we used the cell-free glycolysis system. In this system, we can assume that all the molecules of GAPDH are taking part in the glycolysis, hence we could estimate the GAPDH-AA, according to the kinetic curve (Fig. S8).

We prepared cell lysate from HeLa-siGAPDH and added pure GAPDH into cell lysate to titrate GAPDH-SA. The titrated cell lysate was used for glycolysis assay. In the given range of relative concentration of GAPDH ([GAPDH]) from 0.6 to 1.4, we did not observe a rate of increase of lactate generation (Fig. 7A). [GA3P] was inversely proportional to relative [GAPDH] (Fig. 7B), and the data fit Equation 4. We then calculated the GAPDH-AA, which were virtually the same in the [GAPDH] range between 0.6 and 1.4 (Fig. 7C), quantitatively explaining why titration of GAPDH did not change the lactate generation rate.

Glycolysis and GAPDH in cancer cells

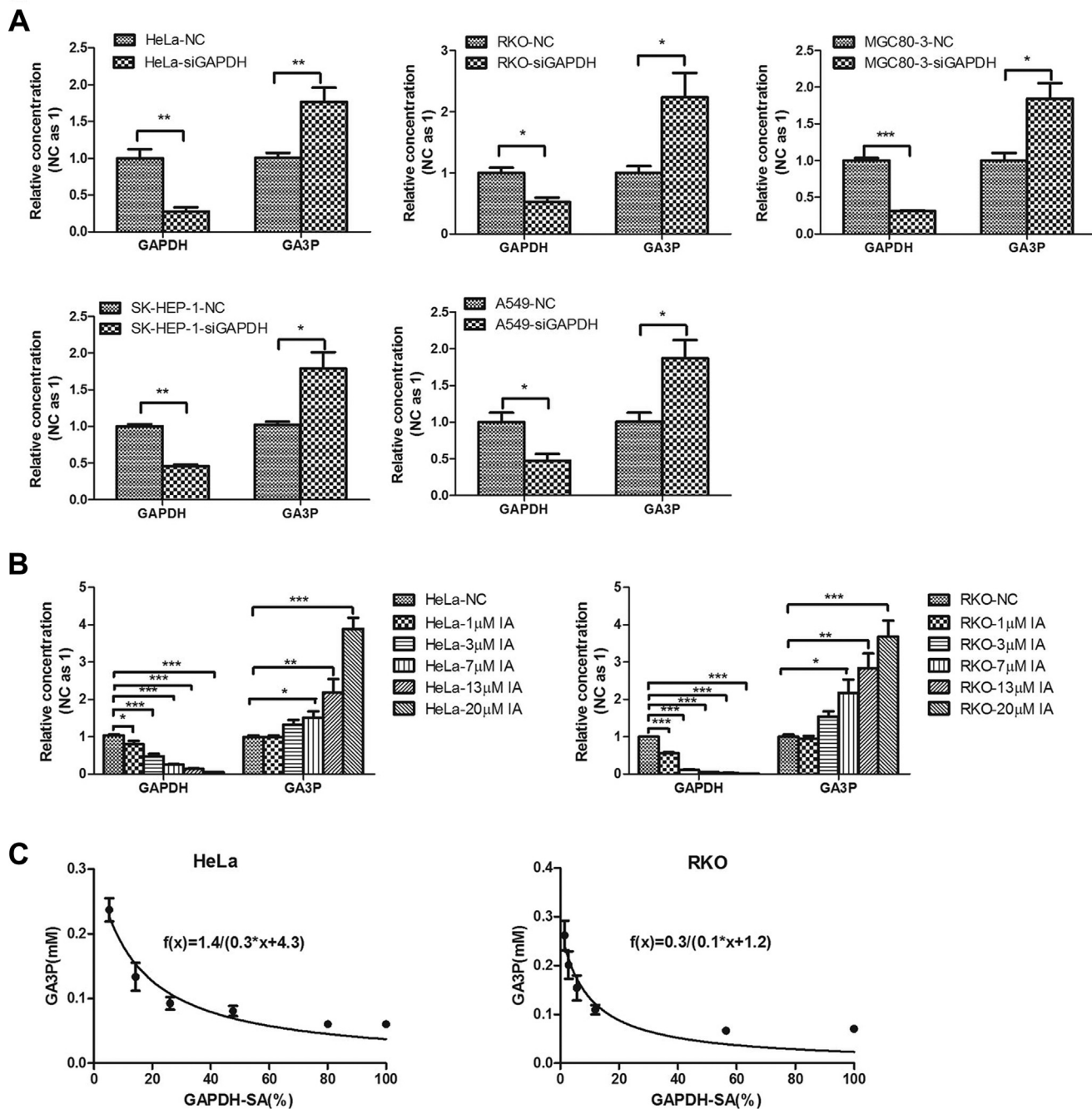


Figure 6. Reciprocal relationship of the relative concentrations between GAPDH and GA3P. A, the relative GAPDH concentrations versus the relative GA3P concentration in HeLa, RKO, MGC80-3, SK-Hep-1, and A549 cells in response to GAPDH knockdown. The relative GAPDH concentration was derived according to Equation 1 based on the data in Table S3. The relative GA3P concentrations are derived from Table S4. B, the relative GAPDH concentrations versus the relative GA3P concentration in HeLa and RKO cells treated with IA at the indicated concentrations. The relative GAPDH concentrations are derived from Table S5, and the relative GA3P concentrations are derived from Table S6. C, [GA3P] as a function of GAPDH-SA as the variable. * $p < 0.05$ and ** $p < 0.01$ by two-tailed Student's t test for panel A. * $p < 0.05$, ** $p < 0.01$, and *** $p < 0.001$ by one-way ANOVA with Dunnett's multiple comparison for panel B. Data are the mean \pm SEM from three independent experiments. GAPDH-SA, GAPDH specific activity; GA3P, glyceraldehyde 3-phosphate.

We then prepared cell lysate from HeLa cells pretreated with IA, which inhibited GAPDH-SA by 95%. The cell lysate was titrated by GAPDH and was used for cell-free glycolysis assay. We correlated the lactate generation with GAPDH-SA (Fig. 7D). The quantitative relationship is similar to that in the cells, that is, it could be expressed by two functions, $f(x) = c$ when GAPDH-SA % is between 40% and 100% and $f(x) = ax / (b + x)$ when GAPDH-

SA% was below 40%. The reciprocal quantitative relationship between [GA3P] and GAPDH-SA% fits Equation 4 very well (Fig. 7E).

Then, we calculated the GAPDH-AA and correlated GAPDH-AA with GAPDH-SA (Fig. 7F). From Figure 7, D and E, we could see that when GAPDH-SA% ranged from 100% to 40%, the lactate generation rate was a constant and GAPDH-

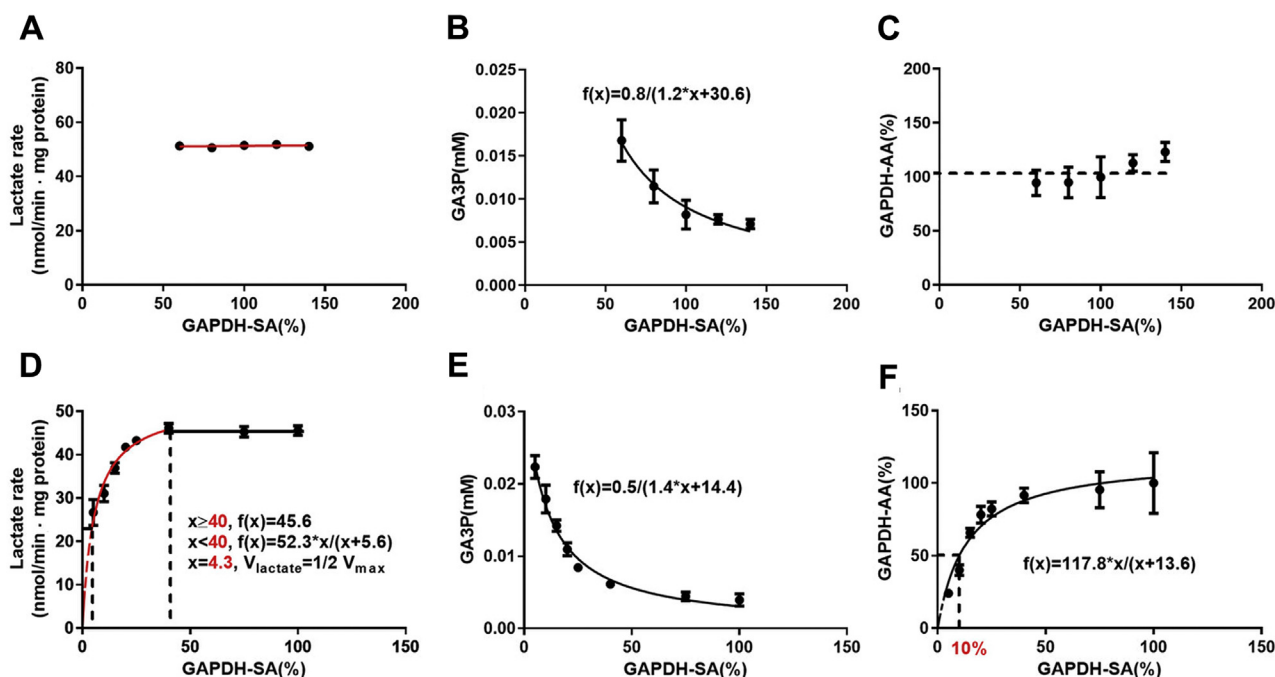


Figure 7. Correlating lactate generation rate with GAPDH-AA. A–C, the lactate generation rate versus GAPDH-SA; [GA3P] in the glycolysis flux versus GAPDH-SA; GAPDH-AA (GAPDH-AA at the [GA3P] in the glycolysis flux) versus GAPDH-SA. Cell lysate was prepared from HeLa_{siGAPDH} and titrated with pure GAPDH. The GAPDH titrated cell lysate was used for cell-free glycolysis assay as described in [Experimental procedures](#). [GA3P] are from [Table S7](#), GAPDH-AA are from [Table S8](#). D, the lactate generation rate versus GAPDH-SA. Cell lysate was prepared from HeLa cells treated with 20 μM IA for 5 h and titrated with pure GAPDH. The GAPDH-titrated cell lysate was used for cell-free glycolysis assay as described in [Experimental procedures](#). When GAPDH-SA is from 100% to 40%, $V = C$; when GAPDH-SA is less than 40%, $V = ax/(b+x)$, where x refers to GAPDH-SA%; $1/2 V_{\text{max}}$ corresponds to GAPDH-SA at 4.3%. E, the [GA3P] as the function of GAPDH-SA as the variable. F, the GAPDH-AA versus GAPDH-SA. 50% GAPDH-AA corresponds to 10% GAPDH-SA. [GA3P] is from [Table S9](#), and GAPDH-AA is from [Table S10](#). Data are the mean \pm SEM from three independent experiments. GAPDH-AA, GAPDH actual activity; GAPDH-SA, GAPDH specific activity.

AA was nearly constant. The half lactate generation rate corresponded to 4.3% GAPDH-SA and the estimated 50% GAPDH-AA corresponded to 10% GAPDH-SA. The data demonstrated that GAPDH-AA was in parallel with the lactate generation rate, indicating that the rate through GAPDH in the glycolysis was balanced by both [GAPDH] and [GA3P].

The thermodynamic nature of glycolysis in cancer cells with the Warburg phenotype

The thermodynamic state of glycolysis in five different cancer cell lines share the same pattern ([Fig. S9A](#)).

The Q values ([Table S3](#)) were far smaller than K_{eq} in the reactions catalyzed by HK, PFK1, and PK, generating a large and negative ΔG , which drives the forward flux of glycolysis. The ΔG of the lactate dehydrogenase (LDH)-catalyzed reaction was between -3.4 and -4.1 kJ/mol, favoring the forward reaction, that is, converting pyruvate (Pyr) and NADH to lactate and NAD. This underlies the thermodynamic basis for the WE.

The concentrations of the glycolytic intermediates were controlled by ΔG . The pattern of the glycolytic intermediates could be defined by the Q values or by the concentrations. The intermediates defined by the Q pattern were similar between the five cell lines ([Fig. S9B](#)). As the reactions catalyzed by phosphohexose isomerase (PGI) and aldolase to enolase were in the near-equilibrium state, these enzymes, with high activity, played an important role in maintaining the concentration pattern of the glycolytic intermediates. The near-equilibrium

state of the reactions catalyzed by PGI, triose phosphate isomerase (TPI), and phosphoglycerate mutase (PGAM) well interpreted the three peaks of [G6P], dihydroxyacetone phosphate [DHAP], [3-PG], and the valleys along glycolysis ([Fig. S9C](#)).

The thermodynamic equilibration of glycolysis in cancer cells in response to GAPDH knockdown

Perturbation of GAPDH by siGAPDH did not significantly change the ΔG s of the reactions along the glycolysis pathway in five cancer cell lines ([Fig. S9A](#)), nor the Q pattern of the glycolytic intermediates ([Fig. S9B](#)).

Although [FBP], [DHAP], and [GA3P] were significantly increased in GAPDH-knockdown cells ([Fig. S9C](#)), the Q values of the reactions along the glycolysis did not change significantly, indicating a well-thermodynamic equilibration. It is clear that [GA3P] was controlled by thermodynamic equilibration of [FBP], [DHAP], and [GA3P] altogether.

Taken together, thermodynamics stabilizes the Q pattern of the glycolytic intermediates and controls [GA3P] to maintain a stable rate through GAPDH in glycolysis. This would be further discussed below.

The thermodynamic equilibration of glycolysis and the limit in response to IA inhibition

The approach of the siRNA knockdown is limited by the knockdown efficiency, which has the maximal efficiency of

Glycolysis and GAPDH in cancer cells

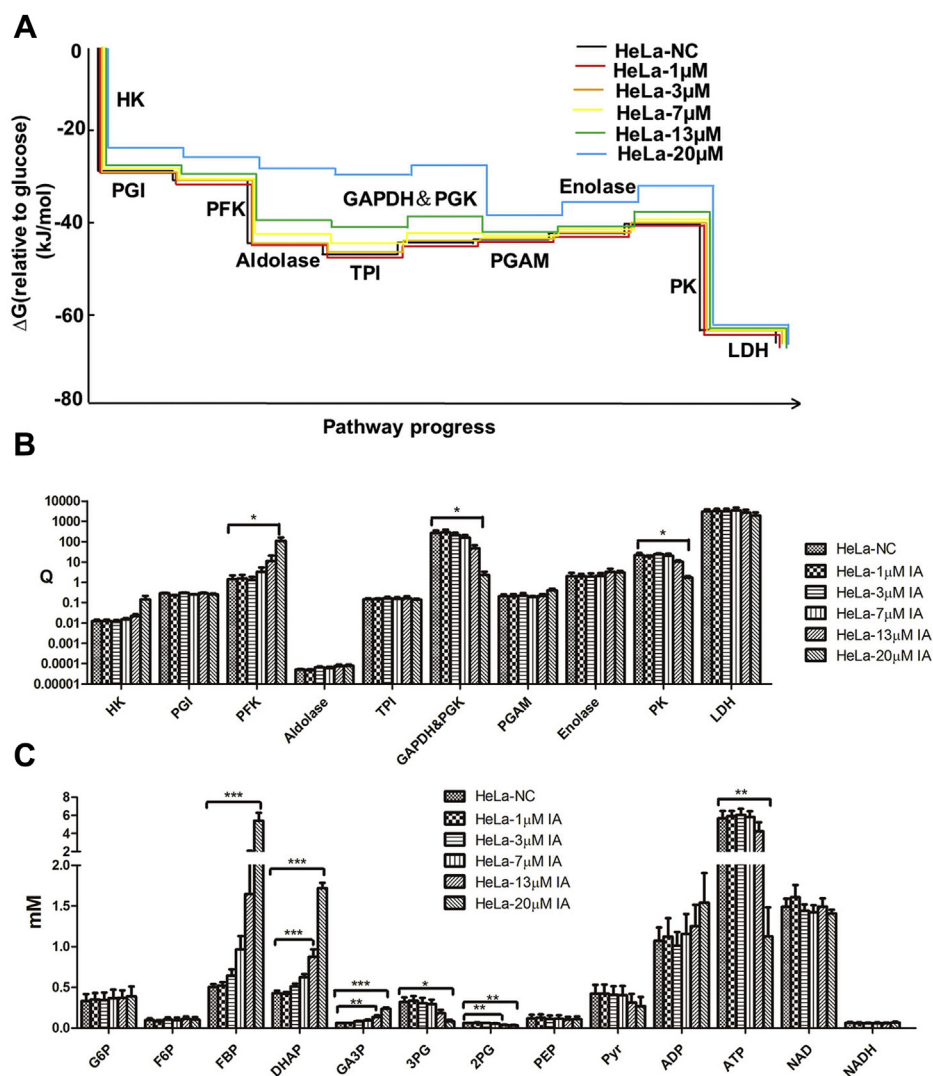


Figure 8. Thermodynamic state of glycolysis and the pattern of the glycolytic intermediates in HeLa cells with or without IA treatment. HeLa cells were treated with IA for 5 h and collected for measurement of cellular glycolytic intermediates and calculation of Q_s and ΔG_s as described in [Experimental procedures](#). A, cumulative ΔG of the reactions along the glycolysis in cancer cells. B, Q patterns of the glycolytic intermediates. C, the concentrations of the glycolytic intermediates. Data in panels A and B are from [Table S5](#). Data in panel C are from [Table S6](#). * $p < 0.05$, ** $p < 0.01$, and *** $p < 0.001$ by one-way ANOVA with Dunnett's multiple comparison. Data are the mean \pm SEM from three independent experiments. IA, iodoacetate.

72% GAPDH knockdown (HeLa) in our experiments. On the other hand, IA could achieve stepwise inhibition of GAPDH-SA in cells. We sought to investigate to what extent inhibition of GAPDH would affect the thermodynamic state of glycolysis.

The $\Sigma\Delta G_s$ (from Glc to lactate) of glycolysis in HeLa cells was not affected by IA ([Fig. 8A](#)). The ΔG_s of each reaction along the pathway were not significantly affected by IA at concentrations between 1 and 7 μM . Although [FBP], [DHAP], and [GA3P] were proportional to the IA concentration ([Fig. 8C](#)), the Q pattern of the glycolytic intermediates was stable ([Fig. 8B](#)). The results therefore demonstrated that all the intermediates were well equilibrated thermodynamically.

The thermodynamic equilibration of the intermediates has a limit. The ΔG_s of PFK1 and GAPDH + PGK1 in the glycolysis significantly changed in HeLa cells treated with 13 and 20 μM IA. We sought to correlate IA with GAPDH ([Fig. 9A](#)) and GAPDH with ΔG of PFK1 or GAPDH + PGK1 ([Fig. 9B](#)).

Notably, the ΔG_s of PFK1 and GAPDH + PGK1 were reciprocally changed, that is, PFK1-catalyzed reaction was approaching the equilibrium state, while GAPDH + PGK1-catalyzed reaction was moving away from the equilibrium state.

Then how to interpret the reciprocal change of the ΔG_s of the reactions catalyzed by PFK1 and GAPDH + PGK1? IA at 13 and 20 μM for 5 h reduced glycolysis by 16% and 61.8%, respectively ([Fig. 4E](#)). Blocking the step of GAPDH in the glycolysis led to reduced [ATP] and [3PG] but increased [ADP], [FBP], and [GA3P] ([Fig. 9C](#)). The [F6P], [NAD], and [NADH] were not significantly changed. As a result, the Q values ($[\text{NADH}][\text{ATP}][\text{3PG}]/([\text{NAD}][\text{ADP}][\text{GA3P}][\text{P}_i])$) of GAPDH + PGK1 were reduced ([Fig. 9D](#), right panel) because of the decreased [ATP]/[ADP] and the decreased [3PG]/[GA3P] ([Fig. 9D](#), left panel). We assumed that [P_i] was a constant. The constant [NADH]/[NAD] was probably balanced by the high activity of LDH in the glycolysis. Thus, the changes of

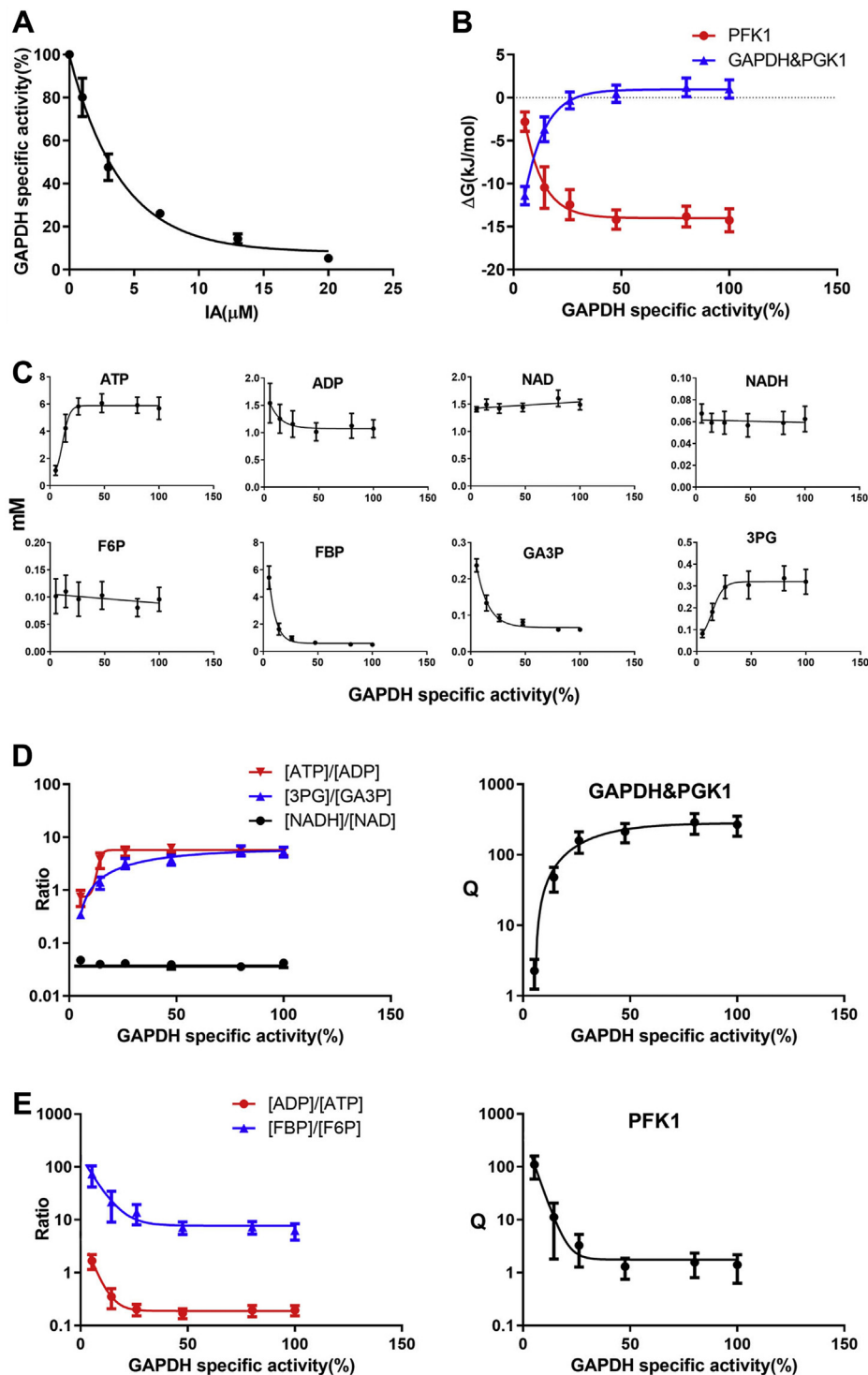


Figure 9. Correlating Δ Gs of the reactions catalyzed by PFK1 and GAPDH + PGK1 with GAPDH-SA in HeLa cells treated with IA. HeLa cells were the same as in Figure 8. *A*, correlating GAPDH-SA with IA. *B*, correlating Δ Gs of the reactions catalyzed by PFK1 and GAPDH + PGK1 with GAPDH-SA. *C*, correlating cellular [ATP], [ADP], [NAD], [NADH], [FBP], [F6P], [GA3P], and [3PG] with GAPDH-SA. *D*, *left panel*, correlating the pairs of the substrate/product of the reactions catalyzed by GAPDH + PGK1 with GAPDH-SA. These pairs of substrate/products compose the Q of the reactions. *Right panel*, correlating Q of the reactions with GAPDH-SA. *E*, *left panel*, correlating the pairs of the substrate/product of the reactions catalyzed by PFK1 with GAPDH-SA. These pairs of substrate/products compose the Q of the reaction. *Right panel*: correlating Q of the reaction with GAPDH-SA. Δ Gs and Qs are from Table S5. The intermediate concentrations and ratios of the substrate/products are from Table S6. Data are the mean \pm SEM from three independent experiments. GAPDH-SA, GAPDH specific activity; IA, iodoacetate.

Glycolysis and GAPDH in cancer cells

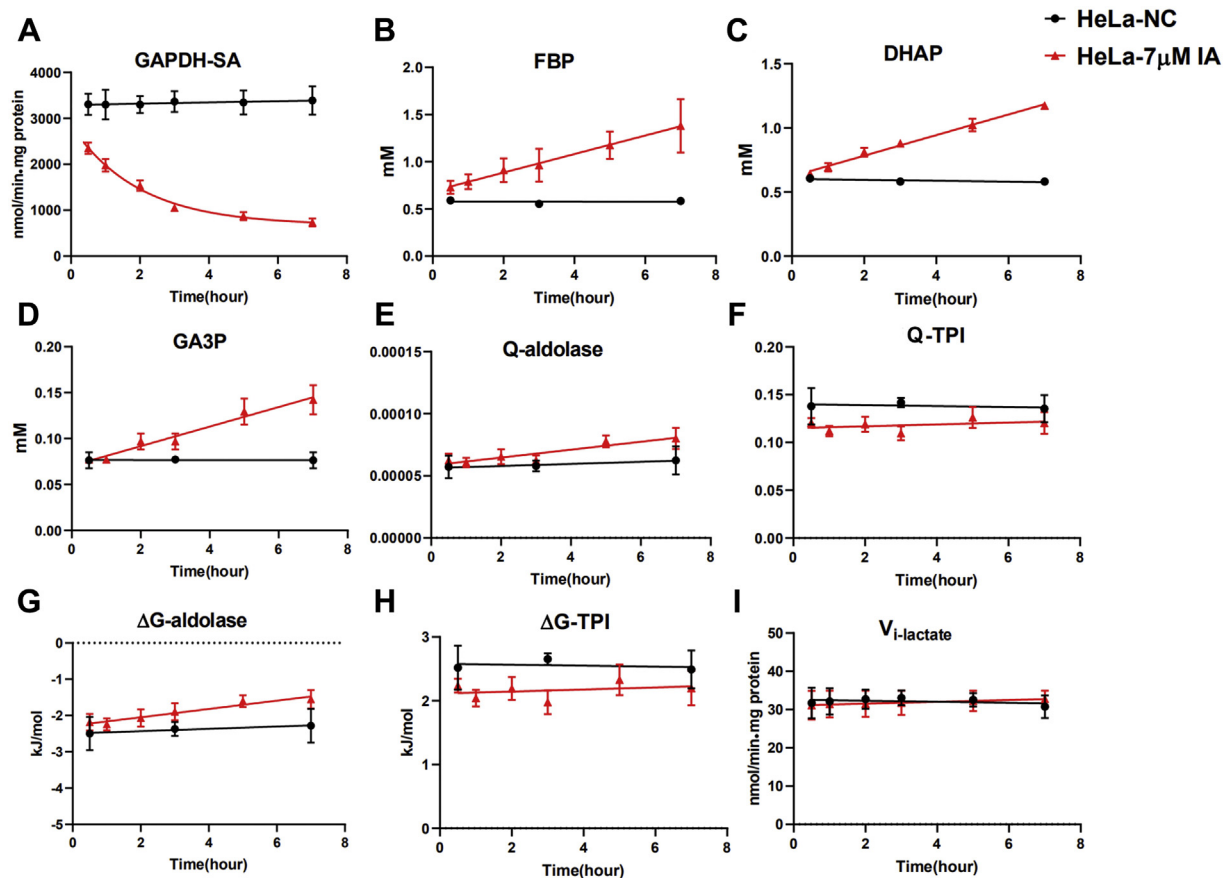


Figure 10. The constant thermodynamic equilibration of glycolysis intermediates in response to IA inhibition. HeLa cells were treated with 7 μM IA for a time course of 7 h. At each interval, cells were collected for measurement of cellular glycolytic intermediates and calculation of Q_s and ΔG_s as described in [Experimental procedures](#). *A*, GAPDH activity. *B–D*, the concentrations of intracellular FBP, DHAP, and GA3P. *E* and *F*, Q values of the corresponding reactions. *G* and *H*, ΔG_s of the corresponding reactions. *I*, the instantaneous rate of lactate generation. Data are the mean \pm SEM from three independent experiments. DHAP, dihydroxyacetone phosphate; FBP, fructose 1,6-bisphosphate; GA3P, glyceraldehyde 3-phosphate; IA, iodoacetate.

[ATP]/[ADP] and [3PG]/[GA3P] were accountable to the change of the ΔG of the reaction catalyzed by GAPDH + PGK1. The change of ΔG of PFK1 in the glycolysis induced by IA was due partly to the increase of [ADP]/[ATP] and partly to the increase of [FBP]/[F6P] (Fig. 9E).

Combining [Figures 4](#) and [8](#) and [Table 1](#), we could clearly see that when GAPDH-SA% was above the critical point, the glycolysis rate was not affected, the concentrations of the intermediates could be well equilibrated thermodynamically, and [GA3P] through thermodynamic equilibration could counter the effect of GAPDH knockdown or inhibition; when GAPDH was inhibited beyond the critical point, the glycolysis rate was inhibited and [GA3P] through thermodynamic equilibration could not fully counter the effect of GAPDH inhibition; as a result, the GAPDH + PGK1-catalyzed reactions were moving away from the near-equilibrium state and became a rate controller.

We used RKO to repeat the above experiment. The results were similar to those derived from HeLa cells (Fig. S10).

We checked if there was a reciprocal change of ΔG_s between the reactions catalyzed by PFK1 and by GAPDH +

PGK1 in GAPDH-knockdown cancer cells. The data demonstrated that there was such a tendency (Fig. S11).

The constant thermodynamic equilibration of glycolysis in cancer cells in response to IA inhibition

We sought to demonstrate the constant thermodynamic equilibration of glycolytic intermediates by a time-course experiment. HeLa cells were treated with 7 μM IA. GAPDH-SA was decreasing in the time course (Fig. 10A), whereas [FBP], [DHAP], [GA3P] were increasing (Fig. 10, B–D). Q values and ΔG_s of the corresponding reactions kept nearly identical, indicating a constant thermodynamic equilibration of the intermediates in the time course (Fig. 10, E–H). The concentrations of other glycolytic intermediates did not change significantly (Fig. S12).

The lactate generation rates of both control and IA treatment kept the same throughout the time course (Fig. 10I).

Collectively, a constant thermodynamic equilibration of intermediates responding to GAPDH inhibition was observed. The constant lactate generation rate indicated a constant rate through GAPDH. Mechanistically, [GA3P] was constantly

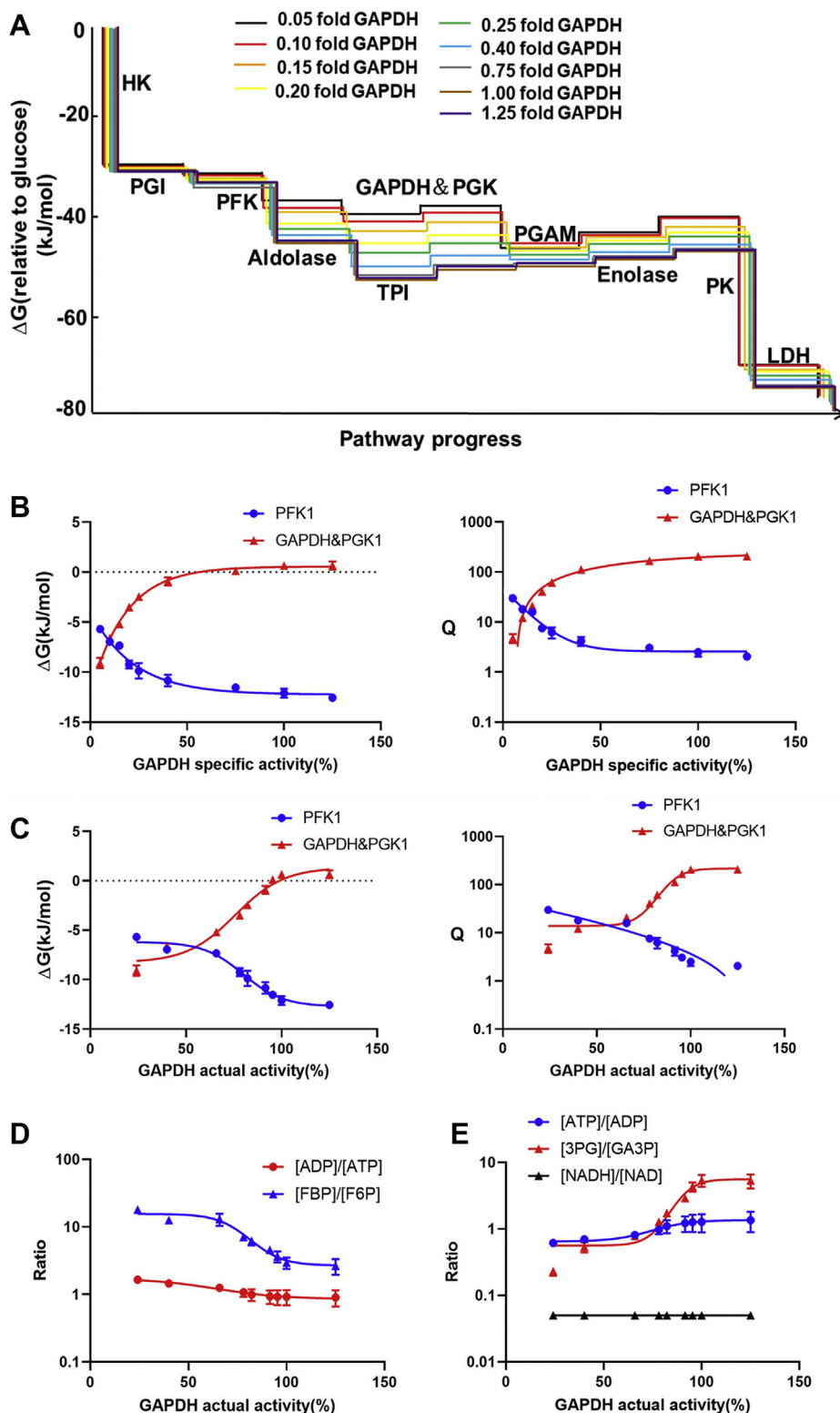


Figure 11. Thermodynamic state of glycolysis in cell-free glycolysis. The cell lysate was prepared from HeLa cells treated with 20 μM IA for 5 h and titrated with pure GAPDH. The GAPDH-titrated cell lysate was used for the cell-free glycolysis assay as described in [Experimental procedures](#). **A**, cumulative ΔG s of the reactions along the glycolysis. **B**, ΔG s and Q s of the reactions catalyzed by PFK1 and GAPDH + PGK1 versus GAPDH-SA. **C**, ΔG s and Q s of the reactions catalyzed by PFK1 and GAPDH + PGK1 versus GAPDH-AA. **D** and **E**, the ratios of the substrate/products versus GAPDH-AA. ΔG s and Q s are from [Table S11](#). The ratios of the substrate/products are from [Table S9](#). Data are the mean \pm SEM from three independent experiments. GAPDH-AA, GAPDH actual activity; IA, iodoacetate.

Glycolysis and GAPDH in cancer cells

regulated by the thermodynamics in the glycolysis pathway, and it was crucial for stabilizing the glycolysis rate.

The thermodynamic state of glycolysis—cell-free glycolysis model

As glycolysis is a part of the metabolic network in living cells, the thermodynamic state of glycolysis is not independent of the network. Using cell-free glycolysis model, we were able to isolate the thermodynamic state of the glycolysis.

We prepared cell lysate from HeLa cells treated with 20 μM IA, which inhibited GAPDH-SA by 95%. The cell lysate was titrated with pure GAPDH and used for glycolysis assay.

The overall thermodynamic state of the glycolysis in the cell-free system (control, *i.e.*, GAPDH-SA 100%) was virtually the same as that in the living cells (Fig. 11A), except at the step of aldolase, which generated a ΔG of -7.71 kJ/mol, while it was -1.84 kJ/mol in living HeLa cells. (Table S5 and S11).

Decrement of GAPDH-SA reduced the negative value of the ΔG s of the reactions catalyzed by PFK1 and aldolase, that is, the reactions were approaching thermodynamic equilibrium (Fig. 11A). On the other hand, decrement of GAPDH-SA increased the negative value of the ΔG of the reaction catalyzed by GAPDH + PGK1 (Fig. 11A), indicating that the reaction was moving away from the thermodynamic equilibrium.

When correlating the GAPDH-SA with the ΔG s or Qs of these reactions (Fig. 11B), the curves were hyperbolic and the changes of ΔG s or Qs correlated with GAPDH-SA% between 40% and 5%. When correlating the change of ΔG s or Qs with GAPDH-AA (Fig. 11C), the curves became sigmoidal and the change of ΔG s or Qs mainly correlated with the GAPDH-AA% between 100% and 75%.

To explain the change of ΔG s, we dissected the Q values into pairs of substrates and products. The reduced negative value of the ΔG (PFK1) was due mainly to $[\text{FBP}]/[\text{F6P}]$ (Fig. 11D), whereas the increased negative value of the ΔG (GAPDH + PGK1) was due mainly to $[\text{3PG}]/[\text{GA3P}]$ (Fig. 11E). This was different from those in living cells, where $[\text{ADP}]/[\text{ATP}]$ or $[\text{ATP}]/[\text{ADP}]$ also contributed to the change of the ΔG s of the reactions catalyzed by PFK1 and GAPDH + PGK1.

We also repeated the experiment using cell lysate prepared from HeLa_{sigGAPDH}. In the range of $[\text{GAPDH}]$ between 0.6 and 1.4, the ΔG s and Qs of the reactions along glycolysis were not significantly different from each other, except that the values of the ΔG of the reaction catalyzed by the PFK1 became less negative, whereas that by GAPDH + PGK1 became more negative (Fig. S13).

Collectively, the thermodynamic state of the glycolysis in the cell-free glycolysis system was virtually the same as that in the living cells, except at the step of aldolase. The effect of perturbation of GAPDH on the thermodynamic state of the glycolysis in the cell-free glycolysis was also similar to that in living cells, except that $[\text{ADP}]/[\text{ATP}]$ played a more important role in the latter than the former.

Discussion

In summary, based on the detailed quantitative data, we deduced the numerical relationship between GAPDH and

glycolysis in cancer cells with the Warburg phenotype, revealed the role of thermodynamics in equilibrating glycolytic intermediates in response to GAPDH perturbation, and interpreted the GAPDH rate through glycolysis flux when GAPDH was perturbed, hence revealed the mechanistic insight into the effect of perturbing GAPDH on the WE. These issues have not been addressed by the previous works. Our work, in line with previous reports (6–8, 15–19), may rationally interpret the efficacy of GAPDH inhibitors with respect to the potential in cancer therapy.

The publications on the WE had been accumulated more than 50,000 by the year of 2016 (30). The tremendous effort has brought a remarkable progress in understanding the WE. Nevertheless, quantification wise is somehow overlooked, given the fact that the quantification is often expressed by the fold change. Without quantification of the variables, the relationship between the variables could not be connected to formulate equations. To the best of our knowledge, our submission represents the first study that deciphered the numerical relationship between the aerobic glycolysis and an individual glycolytic enzyme.

In addition, we would further discuss the role of thermodynamics in glycolysis and the specificity of GAPDH inhibitor for therapeutics purpose.

The role of thermodynamics in glycolysis

The thermodynamic nature of the glycolysis in cancer cells with the WE has not attracted much attention. Thermodynamics is an integrated part in the glycolysis pathway and it plays crucial role in the intermediate equilibration and rate control.

First, thermodynamics plays an important role in dictating the pattern of glycolytic intermediates in cancer cells with the Warburg phenotype. When glycolysis is at steady state, the reactions of PGI, aldolase, TPI, GAPDH, PGK1, PGAM, and enolase were close to thermodynamic equilibrium, which dictates two things, the stable concentration of each glycolytic intermediate and the stable reaction quotient of each reaction (Fig. 8, Figs. S9 and S10, Tables S3–S6). This is why the patterns of glycolytic intermediates, either expressed by concentrations or by Qs, were nearly identical between different cancer cell lines.

Second, thermodynamics plays a crucial role in constantly equilibrating glycolytic intermediates, when GAPDH is perturbed. When GAPDH was inhibited and the critical point was not reached, glycolytic rate was not significantly reduced. Although $[\text{FBP}]$, $[\text{DHAP}]$, and $[\text{GA3P}]$ were significantly increased, ΔG s of the reactions (including aldolase, TPI, GAPDH, and other glycolytic enzymes) were not significantly changed, nor the $\Sigma\Delta G$ s. (Fig. 8, Figs. S9 and S10, Tables S3–S6).

Finally, thermodynamics plays an important role in stabilizing the rate through GAPDH. Glycolysis rate kept constant when GAPDH-SA was above the critical point, indicating a constant rate through GAPDH (Fig. 4, Figs. S2–S5, Table 1). Meanwhile, there existed a reciprocal relationship between the

GAPDH-SA and [GA3P] (Fig. 6). A plausible explanation is that the increase of [GA3P] compensated the loss of GAPDH. This is not only supported by the fundamental enzyme kinetics but also by a constant GAPDH-AA corresponding to a constant glycolytic rate when GAPDH-SA reduced from 100% to 40% (Fig. 7). [GA3P] is controlled by a constant thermodynamic equilibration of the reactions catalyzed by aldolase and TPI (Fig. 10).

The thermodynamic equilibration in response to GAPDH perturbation has a limit and we propose that this limit is a biochemical basis for the rate control of glycolysis by GAPDH in cancer cells. When GAPDH-SA was inhibited beyond the critical point, GAPDH became a rate controller and its catalyzed reaction was moving away from the thermodynamic equilibrium, favoring the forward reaction. This is in consensus with the classical understanding that the rate-limiting step in a pathway is usually far from thermodynamic equilibrium.

In the previous reports, the accumulation of the glycolytic intermediates upstream of the targeted enzyme such as PKM2, PGK1, GAPDH, PGAM, and so forth (7, 8, 16, 31–33), has been interpreted as a result of glycolysis inhibition, and the interpretation is regarded as a ‘proof of concept.’ Nevertheless, this interpretation could be misleading as it does not take thermodynamics into consideration. In this study, we deciphered that the change of the glycolytic intermediates upstream of GAPDH is an outcome of thermodynamic re-equilibration in response to GAPDH perturbation and it is not necessarily an indicator of glycolysis inhibition. Only when GAPDH-SA is inhibited beyond the critical point, the increased [FBP], [DHAP], and [GA3P] would be associated with the rate change of glycolysis.

The specificity of IA and other GAPDH inhibitors

GAPDH has been recognized as a potential target for treating therapy and modulating immunity (6–8, 15–19) because its catalytic cysteine (residue 152) was a highly reactive nucleophile and hence was sensitive to electrophilic reagents. At physiological conditions, the pK_a of the thiol is 8.3, according to the Henderson-Hasselbalch equation, over 90% thiol is protonated and is at an unreactive state. In contrast, the pK_a of the sulfurhydryl group of catalytic cysteine (cysteine 152) of GAPDH was 6.03 because it is located in the pK_a -lowering microenvironment (34), for example, Polgar reported that cysteine 152 in GAPDH formed an ion pair with a neighboring histidine residue in the active site, leading to the deprotonation of the cysteine sulfurhydryl group (35). When pK_a was 6.03, over 90% of the thiol group of cysteine 152 were deprotonated, making it a highly reactive nucleophile, which is readily reactive to IA, an electrophile. Moreover, Carneiro *et al.* (36) showed that the covalent attachment of IA to the active site of the enzyme occurs as a concerted process and that NAD^+ plays an important role in stabilization of the reagents and transition state. Similarly, the inactivation rate of GAPDH by koningic acid, a GAPDH inhibitor (7, 15), was enhanced by NAD^+ by 200 folds (37). Taken together, the

catalytic cysteine of GAPDH is different from the common thiol group, and the former is highly susceptible to IA. Hence, a low IA concentration ($<25 \mu\text{M}$) could effectively inactivate GAPDH but spare other glycolytic enzymes and cellular GSH.

Other GAPDH inhibitors with potential for treating cancer and modulating immunity include dimethyl fumerate (8), 4-octyl itaconic acid (16), and koningic acid (7, 15). Dimethyl fumerate and 4-itaconic acid are α - β unsaturated carbonyls. The thiolate anion on the cysteine residues of GAPDH reacted with the unsaturated carbonyls *via* nucleophilic addition, while dimethyl fumarate conjugated with the catalytic cysteine residue 152 on GAPDH (8) and 4-octyl itaconic with the cysteine residue 22 on GAPDH (16). Koningic acid reacts with catalytic cysteine of GAPDH with the same chemical reaction mechanism as IA—the nucleophilic substitution and the thiolate anion of cysteine 152 attacking the epoxide moiety of the koningic acid (7, 15, 37, 38).

Collectively, IA, dimethyl fumerate, 4-octyl itaconic acid, and koningic acid are all highly reactive electrophiles; in theory, they can react with not only thiolate anion but also other nucleophilic compounds in cells. Hence, the selectivity of these inhibitors depends on the concentration window, in which the thiolate anion of the catalytic cysteine on the GAPDH is conjugated, whereas thiols of GSH and other enzymes are spared. In our study, the concentration of IA was $<25 \mu\text{M}$, which inactivated GAPDH but did not significantly inhibit other glycolytic enzymes nor depleted cellular GSH. In the same principle, the selective inhibition of GAPDH by KA, dimethyl fumerate, and 4-octyl itaconic acid would also depend on their concentration. KA is so far the best characterized GAPDH inhibitor, which selectively inhibited glycolysis in cancer cells with the WE (7).

Experimental procedures

Cell lines

Human cancer cell lines HeLa, MGC80-3, RKO, SK-HEP-1, and A549 were obtained from the Cell Bank of Type Culture Collection of the Chinese Academy of Science and were cultured in RPMI-1640 medium with 10% fetal bovine serum (FBS). Cells were maintained in a humidified incubator at 37 °C with 5% CO_2 .

Reagents and enzymes

Unless otherwise stated, all reagents were from Sigma, including ADP (#A5285), ATP (#A3377), NAD (#N0632), NADP (#N8035), NADH (#N8129), NADPH (#N7505), Glc (#G8270), glucose 6-phosphate (G6P) (#G7879), fructose 6-phosphate (F6P) (#V900924), GA3P (#G5251), 3-phosphoglycerate (#P8877), 2-phosphoglycerate (#19710), phosphoenolpyruvate (PEP) (#P7001), Pyr (#V900232), lactic acid (#L1750), hexokinase (#H4502), PGI (#P5381), phosphofructokinase (#F0137), aldolase (#A8811), TPI (#T6258), GAPDH (#G2267), phosphoglycerate kinase (PGK) (#P7634), enolase (#E6126), PK (#P7768), LDH (#L2500), glucose-6-phosphate dehydrogenase (G6PDH) (#G8404), α -GPDH (#G6751), GSH (#G4251), GSSG (#G6654), 5,5'-Dithiobis (#D8130), GSH reductase (#G3664), Triton X-100

Glycolysis and GAPDH in cancer cells

(#T6878), sulfosalicylic acid (#S2130), 2-vinylpyridine (#132292), triethanolamine (#T1377), Fructose 1,6-bisphosphate (#F111301) and sodium iodoacetate (#S104897) were from Aladdin (China).

GAPDH knockdown by siRNA

1.5×10^5 Cells were seeded into each well of six-well plates and cultured overnight. On the next day, cells were transfected using Lipofectamine 3000 (Thermo Fisher Scientific) according to manufacturer's protocol, with either negative control (NC) siRNA or siGAPDH (RiboBio). The siRNA sequences were as follows: NC, sense, UUCUCCGAACGUGUCACGU dTdT; antisense, ACGUGACACGUUCGGAGAA dTdT. siGAPDH, sense, GUGUGAACCAUGAGAAGUA dTdT; antisense, UACUUCUCAUGGUUCACAC dTdT. Forty-eight hours after transfection, the culture media were replaced with 2 ml fresh Glc-free RPMI-1640 plus 8 mM Glc. Ten-microliter media was collected at 1, 2, 3, 4, 5, and 6 h and Glc and lactate were determined afterward. Then cells were counted and collected for Western blot, glycolysis enzyme activity assay, or intracellular intermediate determination.

Western blotting

Cells were collected and washed twice with cold PBS and then lysed with M-PER Mammalian Protein Extraction Reagent (Thermo Fisher Scientific) supplemented with cocktail (MedChemExpress). The protein concentration was determined with the BCA protein assay kit (Thermo Fisher Scientific). The protein was heat-denatured, and 20 μ g was subjected to 12% SDS-PAGE, transferred to a polyvinylidene fluoride membrane, and incubated with antibodies and then detected by Western lightning plus ECL (Perkin Elmer). The antibodies were GAPDH (Proteintech, #60004-1-Ig) and β -actin (Cell Signaling Technology, #3700).

Inhibition of GAPDH by IA

Cells were seeded into six-well plates and cultured overnight, the seeded numbers for each well of HeLa, RKO, MGC80-3, SK-HEP-1, and A549 were 4.0×10^5 , 7.0×10^5 , 7.0×10^5 , 6.0×10^5 , and 5.0×10^5 , respectively. On the next day, IA was dissolved in water and diluted to different concentrations with 1.5 ml fresh Glc-free RPMI-1640 plus 6 mM Glc. Then, the culture media were replaced with the prepared media above, 10 μ l media and cells were collected at 0.5, 1, 2, 3, 5, and 7 h. Glc and lactate were determined afterward, and cells were counted and lysed for the glycolysis enzyme activity assay.

Cell growth assay

Cells were seeded into six-well plates and cultured overnight, the seeded numbers for each well of HeLa and RKO were 1.5×10^5 and 2.0×10^5 , respectively. On the next day, IA was dissolved in water and diluted to different concentrations with 2.5 ml fresh complete RPMI-1640 plus 10% FBS. Then, the culture medium was replaced and 10 μ l medium was collected at 0, 24, and 48 h. For the cells treated with 8 μ M IA, the culture medium was replaced with 3 ml fresh complete

RPMI-1640 plus 10% FBS (without IA) at 48 h. Then, 10 μ l medium was collected at 72, 96, and 120 h. Glc and lactate were determined afterward, and cells were counted and lysed for the glycolysis enzyme activity assay.

Measurement of Glc and lactate

Glc and lactate were determined according to the methods described previously with some modification (39). Forty microliters of water was added to 10 μ l collected medium and mixed well and then 10 μ l mixture or standard solution of Glc/lactate (LA) was added to the 96-well plate, together with 190 μ l reaction buffer. To determine Glc/LA in cell-free system samples, 10 μ l of the supernatant was added to 190 μ l reaction buffer directly. For Glc determination, the buffer contained 200 mM Hepes (pH 7.4), 100 mM KCl, 5 mM Na_2HPO_4 , 5 mM MgCl_2 , 0.5 mM EDTA, 2 mM ATP, 0.2 mM NADP, 0.2 U/ml HK2, and 0.2 U/ml G6PDH. For lactate determination, the reaction buffer contained 200 mM glycine, 170 mM hydrazine (pH 9.2), 2 mM NAD, and 5 U/ml LDH. Sixty minutes after the reaction, absorbance was recorded at 340 nm using SpectraMax i3 (Molecular Devices). Glc or LA concentration was calculated according to the standard curve.

Determination of intracellular GSH

The content of GSH in cell was determined according to previously reported methods (40), which is essentially a modification of the Tietze recycling assay (41). Briefly, seed the cells at a density of 4.0×10^5 (HeLa cells) per well in a sixwell plate and culture overnight. On the next day, cells were treated with IA at the indicated concentrations for 7 h. Then, cells were counted and suspended in 1 ml of ice-cold extraction buffer (0.1% triton-X and 0.6% sulfosalicylic acid in 0.1 M potassium phosphate buffer with 5 mM EDTA disodium salt, pH 7.5). To ensure that the cells are properly lysed, sonicate the suspension in icy water for 2 to 3 min with vortexing every 30 s. For the measurement of total GSH ($[\text{GSH}] + 2[\text{GSSG}]$), add 20 μ l standards or samples to a 96-well microtiter plate and then mix equal volumes of freshly prepared 5,5'-Dithiobis (2 mg/3 ml) and GSH reductase (3 U/ml) solutions together and add 120 μ l mixed solutions to each well. Allow 30 s for the conversion of GSSG to GSH and then add 60 μ l of β -NADPH (2 mg/3 ml). Immediately read the absorbance at 412 nm in a microplate reader and take measurements every 30 s for 2 min. The rate of change in absorbance ($\Delta A_{412 \text{ nm}} \text{ min}^{-1}$) is linearly proportional to the total concentration of GSH. The concentration of sample is determined by calculating from the regression curve generated from standards of GSH. For the measurement of GSSG, add 100 μ l cell extract to a 1.5 ml Eppendorf tube. Then add 2 μ l 2-vinylpyridine and mix well to derivatize GSH. Allow the reaction to take place for 1 h at room temperature in a fume hood. Add 6 μ l triethanolamine to the side of the tube, and mix the solution vigorously. Assay the derivatized samples by the method described above in a 96-microtitre plate at 412 nm. GSSG standards (containing 2-vinylpyridine and triethanolamine) should also be run.

Glycolysis enzyme activity assay

Cells were collected and lysed with M-PER, and the protein concentration was determined using the BCA protein assay kit. Enzyme activity at the saturating substrate concentration was determined according to previously reported methods (39). Briefly, the reaction buffer contained 200 mM Hepes, 100 mM KCl, 5 mM Na₂HPO₄, 0.5 mM EDTA, and 5 mM MgCl₂, and pH was adjusted to 7.4. For each enzyme activity assay, 1 ml reaction buffer was added to a cuvette and substrates were added as below. The reaction was started by adding cell lysate and mixed, and then absorbance at 340 nm was recorded using a spectrophotometer (DU 700, Beckman Coulter).

HK: 2 mM ATP, 0.2 mM NADP, 10 mM Glc, 1 U/ml G6PDH, 30 µg protein of lysate; PGI: 0.2 mM NADP, 2 mM F6P, 1 U/ml G6PDH; 5 µg protein of lysate; Phosphofructokinase: 2 mM ATP, 0.1 mM ADP, 2 mM F6P, 1 U/ml aldolase, 1 U/ml α-GPDH, 0.1 mM NADH, 10 µg protein of lysate; Aldolase: 1.5 mM fructose 1,6-bisphosphate (FBP), 0.1 mM NADH, 1 U/ml α-GPDH, 15 µg protein of lysate; TPI: 2 mM GA3P, 1 U/ml α-GPDH, 0.1 mM NADH, 1 µg protein of lysate; GAPDH: 2 mM GA3P, 2 mM NAD, 4 µg protein of lysate; PGK: 2 mM 3PG, 2 mM ATP, 1 U/ml GAPDH, 0.1 mM NADH, 5 µg protein of lysate; PGAM: 1 mM 3PG, 2 mM ADP, 1 U/ml enolase, 1 U/ml PK, 1 U/ml LDH, 0.1 mM NADH, 10 µg protein of lysate; Enolase: 1 mM 2PG, 2 mM ADP, 1 U/ml PK, 1 U/ml LDH, 0.1 mM NADH, 10 µg protein of lysate; PK: 2 mM PEP, 2 mM ADP, 5 U/ml LDH, 0.1 mM NADH, 2 µg protein of lysate; LDH: 2 mM Pyr, 0.1 mM NADH, 2 µg protein of lysate.

In vitro cell-free system model for glycolysis

This cell-free model for glycolysis was described by us previously (39, 42). Briefly, a reaction buffer contained 200 mM Hepes, 100 mM KCl, 5 mM Na₂HPO₄, 0.5 mM EDTA, and 5 mM MgCl₂, 1.5 mM ATP, 4 mM ADP, 5 mM Glc, 2 mM NAD, and 0.1 mM NADH was used for the *in vitro* glycolysis system. To start the reaction, 60 µl lysate (8–10 µg/µl protein) was added to 540 µl reaction buffer, and the mixture was incubated at 37 °C. Thirty minutes later, 600 µl 1 M HClO₄ was added to the mixture to terminate the reaction and then 100 µl 3 M K₂CO₃ was added to neutralize, and the mixture was kept on ice for 30 min further. After that, the supernatant was obtained by centrifuging at 10,000g and was used for determination of glycolytic intermediates.

Determination of glycolytic intermediates in the cell-free system

We used previously reported methods to determine the glycolytic intermediates (39). The reaction buffer in this part contained 200 mM Hepes, 100 mM KCl, 5 mM Na₂HPO₄, 0.5 mM EDTA, and 5 mM MgCl₂, with pH adjusted to 7.4.

G6P and F6P: 100 µl of the supernatant and 0.2 mM NADP were added to 900 µl reaction buffer, and the reaction was started by adding 1 U/ml G6PDH. The first reaction to measure G6P ended when 340 nm absorbance reached a plateau, and then, 1 U/ml PGI was added to measure F6P.

FBP, DHAP, and GA3P: 100 µl of the supernatant and 0.1 mM NADH were added to 900 µl reaction buffer; the reaction to measure DHAP was started by adding 1 U/ml α-GPDH. When the first reaction ended, 1 U/ml TPI was added to measure GA3P. Finally, 1 U/ml aldolase was added to measure FBP.

3PG: 50 µl of the supernatant, 2 mM ATP, 0.1 mM NADH, and 1 U/ml PGK were added to 950 µl reaction buffer, and the reaction was started by adding 1 U/ml GAPDH.

2PG, PEP, and Pyr: 100 µl of the supernatant and 0.1 mM NADH were added to 900 µl reaction buffer; the reaction to measure Pyr was started by adding 1 U/ml LDH. When the first reaction ended, 2 mM ADP and 1 U/ml PK were added to measure PEP. Finally, 1 U/ml enolase was added to measure 2PG.

Determination of intracellular glycolytic intermediates

For knockdown experiment, NC or siGAPDH-transfected cells were washed by ice-cold PBS twice, and 600 µl 1 M pre-cold HClO₄ was added to every three wells of a six-well plate. Cells were collected by a scraper, incubated on ice for 30 min, and neutralized by 100 µl 3 M K₂CO₃. Then, the supernatant was obtained by centrifuging at 10,000g at 4 °C. Then, 50 µl 2 M NaOH was added to the supernatant and kept at 60 °C for 5 min and neutralized again by adding 50 µl 2 M HCl. These two steps eliminated intracellular NAD(H)/NADP(H) possibly. Meanwhile, a same fourth well of cells was trypsinized and collected to determine the cell number and cell size by a cell counter (JIMBIO). Through the following reactions, intermediates plus NADP (for G6P, F6P, and Glc) or NADH (for FBP-Pyr) were converted to products and NADPH or NAD; termination of the reaction by NaOH or HCl will conserve the NADPH or NAD, which could be measured by cycling methods (43, 44). For all the reactions, 10 µl supernatant was mixed with 40 µl reaction buffer; different reactions differ in the reaction buffer:

G6P: 200 mM Hepes, 100 mM KCl, 5 mM Na₂HPO₄, 0.5 mM EDTA, 5 mM MgCl₂, pH 7.4, 2 mM ATP, 0.5 mM NADP, 0.5 U/ml G6PDH; F6P: 200 mM Hepes, 100 mM KCl, 5 mM Na₂HPO₄, 0.5 mM EDTA, 5 mM MgCl₂, pH 7.4, 2 mM ATP, 0.5 mM NADP, 0.5 U/ml G6PDH, plus 0.5 U/ml PGI; Glc: 200 mM Hepes, 100 mM KCl, 5 mM Na₂HPO₄, 0.5 mM EDTA, 5 mM MgCl₂, pH 7.4, 2 mM ATP, 0.5 mM NADP, 0.5 U/ml G6PDH, plus 0.5 U/ml HK; DHAP: 200 mM Hepes, 100 mM KCl, 5 mM Na₂HPO₄, 0.5 mM EDTA, 5 mM MgCl₂, pH 7.4, 0.5 mM NADH, 0.5 U/ml α-GPDH; GA3P: 200 mM Hepes, 100 mM KCl, 5 mM Na₂HPO₄, 0.5 mM EDTA, 5 mM MgCl₂, pH 7.4, 0.5 mM NADH, 0.5 U/ml α-GPDH, plus 0.5 U/ml TPI; FBP: 200 mM Hepes, 100 mM KCl, 5 mM Na₂HPO₄, 0.5 mM EDTA, 5 mM MgCl₂, pH 7.4, 0.5 mM NADH, 0.5 U/ml α-GPDH, 0.5 U/ml TPI, plus 0.5 U/ml aldolase; 3PG: 200 mM Hepes, 100 mM KCl, 0.5 mM EDTA, 5 mM MgCl₂, pH 7.4, 0.5 mM NADH, 1 mM ATP, 0.5 U/ml PGK, plus 0.5 U/ml GAPDH; Pyr: 200 mM Hepes, 100 mM KCl, 5 mM Na₂HPO₄, 0.5 mM EDTA, 5 mM MgCl₂, pH 7.4, 0.5 mM NADH, 1 mM ADP, 0.5 U/ml LDH; PEP: 200 mM Hepes, 100 mM KCl, 5 mM Na₂HPO₄, 0.5 mM EDTA, 5 mM MgCl₂, pH 7.4, 0.5 mM NADH, 1 mM ADP, 0.5 U/ml LDH, plus 0.5 U/ml PK; 2PG: 200 mM Hepes, 100 mM KCl, 5 mM Na₂HPO₄, 0.5 mM

Glycolysis and GAPDH in cancer cells

EDTA, 5 mM MgCl₂, pH 7.4, 0.5 mM NADH, 1 mM ADP, 0.5 U/ml LDH, 0.5 U/ml PK, plus 0.5 U/ml enolase.

For G6P, F6P, and Glc determination, after 30 min incubation at 37 °C, the reaction was terminated by adding 10 µl 2 M NaOH, mixed well, and kept at 60 °C for 5 min to eliminate NADP and then the mixture was neutralized by adding 20 µl 1 M HCl. For the rest of the intermediates, after 30 min incubation at 37 °C, the reaction was terminated by adding 20 µl 1 M HCl, kept at 60 °C for 5 min to eliminate NADH, and then the mixture was neutralized by adding 10 µl 2 M NaOH. After that, 70 µl neutralized mixture or standard solution was added to a 96-well plate together with 100 µl development buffer (0.4 M Tris HCl, 0.2 mM G6P, 1 U/ml G6PDH, 0.1 mM methanethiosulfonate, 0.1 mM phenazine ethosulfate, pH 7.8) to cycling NADPH (for G6P, F6P, and Glc). For the rest of the intermediates, the development buffer contained 0.4 M Tris HCl, pH 7.8, 5 M ethanol, 2 U/ml alcohol dehydrogenase, 0.1 mM methanethiosulfonate, 0.1 mM phenazine ethosulfate. After 30 min incubation with the development buffer at 37 °C, the 490 nm absorbance of 96-well plates was recorded and analyzed.

For IA inhibition experiment, NC or IA inhibited cells were washed by ice-cold PBS twice, and 600 µl 1 M precold HClO₄ was added to every three 10 cm dishes. Cells were collected by a scraper, incubated on ice for 30 min, and neutralized by 100 µl 3 M K₂CO₃. After that, the supernatant was obtained by centrifuging at 10,000g and was used for determination of intracellular glycolytic intermediates. The methods were same as determination of glycolytic intermediates in the cell-free system mentioned above.

Determination of ATP, ADP, NAD, and NADH in cells

Cells in six-well plates were washed with ice-cold PBS twice, and 0.6 ml 80% (vol/vol) precold (-20 °C) methanol was added per well to extract the intracellular metabolites. Then a scraper was used to collect the cells, and the cell debris was discarded by centrifuging at 20,000g at 4 °C. The supernatant was evaporated by a vacuum centrifugal concentrator and was dissolved in 100 µl water for following ultra performance liquid chromatography (UPLC) analysis. Waters ACQUITY UPLC system with an ACQUITY UPLC HSS T3 column was used to perform the liquid chromatography. The mobile phase A was 20 mM triethylamine in 99%/1% water/acetonitrile (pH 6.5), and the mobile phase B was 100% acetonitrile. The gradient program was as follows: 0 to 3 min, 100% A; 3 to 4 min, 100% A-98.5% A; 4 to 7 min, 98.5% A- 92% A; 7 to 7.1 min, 92% A-100% A; 7.1 to 10 min, 100% A. Ten microliter sample or standard solution was injected to perform the analysis with a flow rate at 0.3 ml/min. During the performance, the column was kept at 40 °C.

Analysis of isotopic lactate by LC-MS/MS

Isotopic lactate tracing is based on our previously reported method (45). [¹³C₆]Glucose was purchased from Sigma. Forty-eight hours after transfection, HeLa-NC, HeLa-siGAPDH, MGC80-3-NC, and MGC80-3-siGAPDH were washed with PBS twice and cultured in Glc-free RPMI-1640

supplemented with 10% ultrafiltered FBS and 8 mM [¹³C₆] glucose for 6 h. Then, the culture medium was collected and diluted 40 times with 100% acetonitrile and centrifuged at 25,000g for 10 min at 4 °C. The supernatant was collected for LS-MS/MS analysis according to methods reported previously by us (45, 46). Briefly, an ACQUITY BEH Amide column was used to perform liquid chromatography, kept at 50 °C during analysis, and the injection volume was 7.5 µl. Mobile phase A was 10 mM ammonium acetate in 85% acetonitrile and 15% water, pH 9.0, and mobile phase B was 10 mM ammonium acetate in 50% acetonitrile and 50% water, pH 9.0. The gradient program was as follows: 0 to 0.4 min, 100% A; 0.4 to 2 min, 100 to 30% A; 2 to 2.5 min, 30 to 15% A; 2.5 to 3 min, 15% A; 3 to 3.1 min, 15 to 100% A; 3.1 to 7.5 min, 100% A. A 4000 QTRAP mass spectrometer (AB Sciex) equipped with an ESI ion source (Turbo Spray) operated in the negative-ion mode was used for MS detection, and the same parameter setting was used (45).

Calculation of the Gibbs free energy change ΔG of glycolytic reactions

ΔG was calculated according to Equation 5,

$$\Delta G = \Delta G_{310}^{\prime 0} + RT \ln Q \quad (5)$$

where $\Delta G_{310}^{\prime 0}$ is the standard transformed Gibbs free energy at 37 °C and Q was calculated according to intermediate concentrations and is listed in tables. NAD/NADH was set as 78 according to our previously reported study (42) and [Pi] in the cell was 1.5 mM according to (47). Take the HeLa-NC of knock-down experiment *in vivo* for example. Q of HK-catalyzed reaction in cell equals to $[G6P][ADP]/[ATP][Glc]$, which was 0.013; however, $\Delta G_{310}^{\prime 0}$ is not available. According to $\Delta G = \Delta H - T\Delta S$ because the change of ΔH and ΔS is negligible between 37 °C and 25 °C (48, 49), we deduced the equation to a new form as shown in Equation 6,

$$\Delta G_{310}^{\prime 0} = \frac{310}{298} \Delta G_{298}^{\prime 0} + \left(1 - \frac{310}{298}\right) \Delta H_{298}^{\prime 0} \quad (6)$$

$\Delta G_{298}^{\prime 0}$ and $\Delta H_{298}^{\prime 0}$ are available in references (50–54). So we get Equation 7,

$$\begin{aligned} \Delta G &= \frac{310}{298} \Delta G_{298}^{\prime 0} + \left(1 - \frac{310}{298}\right) \Delta H_{298}^{\prime 0} + RT \ln Q = \frac{310}{298} (-16.7) \\ &+ \left(1 - \frac{310}{298}\right) (-23.8) + 8.31 \times 0.31 \times \ln(0.013) \\ &= -27.68 \text{ kJ/mol} \end{aligned} \quad (7)$$

Statistical analysis

All experiments were repeated at least 3 times, and all data were analyzed using GraphPad Prism 7. For comparisons of two groups, two-tailed Student's *t* test was performed. For comparisons of three or more groups, one-way ANOVA was

performed with post hoc multiple comparison testing using Dunnett's method.

Data availability

All the data are in the article.

Supporting information—This article contains [supporting information](#).

Acknowledgments—We thank professor Guo-Hua Fong (University of Connecticut School of Medicine) for critical reading of this manuscript and constructive comments.

Author contributions—X. H. conceived the conception, designed the study, interpreted the data, and wrote the paper. X. Z., C. J., and Q. P. conducted the experiments.

Funding and additional information—This work has been supported in part by the China National 973 project (2013CB911303), China Natural Science Foundation projects (81470126, 82073038), a key project (2018C03009) funded by Zhejiang Provincial Department of Sciences and Technologies, the Fundamental Research Funds for the Central Universities (2017XZZX001-01, 2019FZJD009), and the National Ministry of Education, China, to X. H.

Conflict of interest—The authors declare that they have no conflicts of interest with the contents of this article.

Abbreviations—The abbreviations used are: DHAP, dihydroxyacetone phosphate; F6P, fructose 6-phosphate; FBP, fructose 1,6-bisphosphate; FBS, fetal bovine serum; G6P, glucose 6-phosphate; G6PDH, glucose-6-phosphate dehydrogenase; GA3P, glyceraldehyde 3-phosphate; GAPDH-AA, GAPDH actual activity; GAPDH-SA, GAPDH specific activity; Glc, glucose; HK, hexokinase; IA, iodoacetate; LDH, lactate dehydrogenase; NC, negative control; PEP, phosphoenolpyruvate; PGAM, phosphoglycerate mutase; PGI, phosphohexose isomerase; PGK, phosphoglycerate kinase; PK, pyruvate kinase; Pyr, pyruvate; TPI, triose phosphate isomerase; UPLC, ultra performance liquid chromatography; WE, Warburg effect.

References

- Altman, B. J., Stine, Z. E., and Dang, C. V. (2016) From Krebs to clinic: Glutamine metabolism to cancer therapy. *Nat. Rev. Cancer* **16**, 619–634
- Cascone, T., McKenzie, J. A., Mbofung, R. M., Punt, S., Wang, Z., Xu, C., Williams, L. J., Wang, Z., Bristow, C. A., Carugo, A., Peoples, M. D., Li, L., Karpinets, T., Huang, L., Malu, S., et al. (2018) Increased tumor glycolysis characterizes immune resistance to adoptive T cell therapy. *Cell Metab.* **27**, 977–987.e974
- Nakazawa, M. S., Keith, B., and Simon, M. C. (2016) Oxygen availability and metabolic adaptations. *Nat. Rev. Cancer* **16**, 663–673
- Yang, M., and Vousden, K. H. (2016) Serine and one-carbon metabolism in cancer. *Nat. Rev. Cancer* **16**, 650–662
- Pelicano, H., Martin, D. S., Xu, R. H., and Huang, P. (2006) Glycolysis inhibition for anticancer treatment. *Oncogene* **25**, 4633–4646
- Yun, J., Mullarky, E., Lu, C., Bosch, K. N., Kavalier, A., Rivera, K., Roper, J., Chio, I. I., Giannopoulos, E. G., Rago, C., Muley, A., Asara, J. M., and Paik, J. (2015) Vitamin C selectively kills KRAS and BRAF mutant colorectal cancer cells by targeting GAPDH. *Science* **350**, 1391–1396
- Liberti, M. V., Dai, Z., Wardell, S. E., Baccile, J. A., Liu, X., Gao, X., Baldi, R., Mehrmohamadi, M., Johnson, M. O., Madhukar, N. S., Shestov, A. A., Chio, I. I. C., and Elemento, O. (2017) A predictive model for selective targeting of the Warburg effect through GAPDH inhibition with a natural product. *Cell Metab.* **26**, 648–659
- Kornberg, M. D., Bhargava, P., Kim, P. M., Putluri, V., Snowman, A. M., Putluri, N., Calabresi, P. A., and Snyder, S. H. (2018) Dimethyl fumarate targets GAPDH and aerobic glycolysis to modulate immunity. *Science* **360**, 449–453
- Van Schaftingen, E., Hue, L., and Hers, H. G. (1980) Fructose 2,6-bisphosphate, the probably structure of the glucose- and glucagon-sensitive stimulator of phosphofructokinase. *Biochem. J.* **192**, 897–901
- Okar, D. A., Manzano, A., Navarro-Sabate, A., Riera, L., Bartrons, R., and Lange, A. J. (2001) PFK-2/FBPase-2: Maker and breaker of the essential biofactor fructose-2,6-bisphosphate. *Trends Biochem. Sci.* **26**, 30–35
- Ashizawa, K., Willingham, M. C., Liang, C. M., and Cheng, S. Y. (1991) *In vivo* regulation of monomer-tetramer conversion of pyruvate kinase subtype M2 by glucose is mediated via fructose 1,6-bisphosphate. *J. Biol. Chem.* **266**, 16842–16846
- Chaneton, B., Hillmann, P., Zheng, L., Martin, A. C. L., Maddocks, O. D. K., Chokkathukalam, A., Coyle, J. E., Jankevics, A., Holding, F. P., Vousden, K. H., Frezza, C., O'Reilly, M., and Gottlieb, E. (2012) Serine is a natural ligand and allosteric activator of pyruvate kinase M2. *Nature* **491**, 458–462
- Ardehali, H., Yano, Y., Printz, R. L., Koch, S., Whitesell, R. R., May, J. M., and Granner, D. K. (1996) Functional organization of mammalian hexokinase II - Retention of catalytic and regulatory functions in both the NH₂- and COOH-terminal halves. *J. Biol. Chem.* **271**, 1849–1852
- Dai, Z., and Locasale, J. W. (2018) Thermodynamic constraints on the regulation of metabolic fluxes. *J. Biol. Chem.* **293**, 19725–19739
- Shestov, A. A., Liu, X., Ser, Z., Cluntun, A. A., Hung, Y. P., Huang, L., Kim, D., Le, A., Yellen, G., Albeck, J. G., and Locasale, J. W. (2014) Quantitative determinants of aerobic glycolysis identify flux through the enzyme GAPDH as a limiting step. *eLife* **3**
- Liao, S., Han, C., Xu, D., Fu, X., Wang, J., and Kong, L. (2019) 4-Octyl itaconate inhibits aerobic glycolysis by targeting GAPDH to exert anti-inflammatory effects. *Nat. Commun.* **10**
- Liberti, M. V., Allen, A. E., Ramesh, V., Dai, Z., Singleton, K. R., Guo, Z., Liu, J. O., Wood, K. C., and Locasale, J. W. (2020) Evolved resistance to partial GAPDH inhibition results in loss of the Warburg effect and in a different state of glycolysis. *J. Biol. Chem.* **295**, 111–124
- Zhong, X. Y., Yuan, X. M., Xu, Y. Y., Yin, M., Yan, W. W., Zou, S. W., Wei, L. M., Lu, H. J., Wang, Y. P., and Lei, Q. Y. (2018) CARM1 methylates GAPDH to regulate glucose metabolism and is suppressed in liver cancer. *Cell Rep.* **24**, 3207–3223
- Locasale, J. W. (2018) New concepts in feedback regulation of glucose metabolism. *Curr. Opin. Syst. Biol.* **8**, 32–38
- Jin, C., Zhu, X., Wu, H., Wang, Y., and Hu, X. (2020) Perturbation of phosphoglycerate kinase 1 (PGK1) only marginally affects glycolysis in cancer cells. *J. Biol. Chem.* **295**, 6425–6446
- Williamson, J. R. (1967) Glycolytic Control Mechanisms III. Effects of iodoacetamide and fluoroacetate on glucose metabolism in the perfused rat heart. *J. Biol. Chem.* **242**, 4476–4485
- Campbell-Burk, S. L., Jones, K. A., and Shulman, R. G. (1987) 31P NMR saturation-transfer measurements in *Saccharomyces cerevisiae*: Characterization of phosphate exchange reactions by iodoacetate and antimycin A inhibition. *Biochemistry* **26**, 7483–7492
- Sabri, M. I., and Ochs, S. (1971) Inhibition of glyceraldehyde-3-phosphate dehydrogenase in mammalian nerve by iodoacetic acid. *J. Neurochem.* **18**, 1509–1514
- Schmidt, M. M., and Dringen, R. (2009) Differential effects of iodoacetamide and iodoacetate on glycolysis and glutathione metabolism of cultured astrocytes. *Front. in Neuroenergetics* **1-1**
- Lambeir, A. M., Loiseau, A. M., Kuntz, D. A., Vellieux, F. M., Michels, P. A., and Opperdoes, F. R. (1991) The cytosolic and glycosomal glyceraldehyde-3-phosphate dehydrogenase from *Trypanosoma brucei* Kinetic properties and comparison with homologous enzymes. *Eur. J. Biochem.* **198**, 429–435
- Mountassif, D., Baibai, T., Fourrat, L., Moutaouakkil, A., Iddar, A., El Kebba, M. S., and Soukri, A. (2009) Immunoaffinity purification and

Glycolysis and GAPDH in cancer cells

- characterization of glyceraldehyde-3-phosphate dehydrogenase from human erythrocytes. *Acta Biochim. Biophys. Sinica* **41**, 399–406
27. Daniela, A. S., Ellen, K. S., Leonor, C. A. S., and Calderon-Aranda, E. S. (2011) Role of nitric oxide produced by inos through nf-kb pathway in migration of cerebellar granule neurons induced by lipopolysaccharide. *Cell. Signal.* **23**, 425–435
 28. Hara, M. R., Agrawal, N., Kim, S. F., Cascio, M. B., Fujimuro, M., Ozeki, Y., Takahashi, M., Cheah, J. H., Tankou, S. K., Hester, L. D., Ferris, C. D., Hayward, S. D., Snyder, S. H., and Sawa, A. (2005) S-nitrosylated GAPDH initiates apoptotic cell death by nuclear translocation following Siah1 binding. *Nat. Cell Biol* **7**, 665–674
 29. Tarze, A., Deniaud, A., Bras, M. L., Maillier, E., Molle, D., Larochette, N., and Brenner, C. (2007) GAPDH, a novel regulator of the pro-apoptotic mitochondrial membrane permeabilization. *Oncogene* **26**, 2606–2620
 30. Liberti, M. V., and Locasale, J. W. (2016) The Warburg effect: How does it benefit cancer cells? *Trends Biochem. Sci.* **41**, 211–218
 31. Anastasiou, D., Pouligiannis, G., Asara, J. M., Boxer, M. B., Jiang, J., Shen, M., and Cantley, L. C. (2011) Inhibition of pyruvate kinase M2 by reactive oxygen species contributes to cellular antioxidant responses. *Science* **334**, 1278–1283
 32. Hitosugi, T., Zhou, L., Elf, S., Fan, J., Kang, H. B., Seo, J. H., and Chen, J. (2012) Phosphoglycerate mutase 1 coordinates glycolysis and biosynthesis to promote tumor growth. *Cancer Cell* **22**, 585–600
 33. Shi, Y., Vaden, D. L., Ju, S., Ding, D., Geiger, J. H., and Greenberg, M. L. (2005) Genetic perturbation of glycolysis results in inhibition of de novo inositol biosynthesis. *J. Biol. Chem.* **280**, 41805–41810
 34. Martyniuk, C. J., Fang, B., Koomen, J. M., Gavin, T., LoPachin, R. M., and Barber, D. S. (2011) Molecular mechanisms of α,β -unsaturated carbonyl toxicity: Cysteine-adduct formation correlates with loss of enzyme function. *Chem. Res. Toxicol.* **24**, 2302–2311
 35. Polgar, L. (1975) Ion-pair formation as a source of enhanced reactivity of the essential thiol group of d-glyceraldehyde-3-phosphate dehydrogenase. *FEBS J.* **51**, 63–71
 36. Carneiro, A. S., Lameira, J., and Alves, C. N. (2011) A theoretical study of the molecular mechanism of the GAPDH Trypanosoma cruzi enzyme involving iodoacetate inhibitor. *Chem. Phys. Lett.* **514**, 336–340
 37. Sakai, K., Hasumi, K., and Endo, A. (1988) Inactivation of rabbit muscle glyceraldehyde-3-phosphate dehydrogenase by koniginic acid. *Biochim. Biophys. Acta* **952**, 297–303
 38. Sakai, K., Hasumi, K., and Endo, A. (1990) Two glyceraldehyde-3-phosphate dehydrogenase isozymes from the koniginic acid (heptelidic acid) producer *Trichoderma koniginii*. *FEBS J.* **193**, 195–202
 39. Passonneau, J. V., and Lowry, O. H. (1993) *Enzymatic Analysis: A Practical Guide*, Humana Press, Totowa, NJ
 40. Rahman, I., Kode, A., and Biswas, S. K. (2006) Assay for quantitative determination of glutathione and glutathione disulfide levels using enzymatic recycling method. *Nat. Protoc.* **1**, 3159–3165
 41. Tietze, F. (1969) Enzymic method for quantitative determination of nanogram amounts of total and oxidized glutathione: Applications to mammalian blood and other tissues. *Anal. Biochem.* **27**, 502–522
 42. Xie, J., Dai, C., and Hu, X. (2016) Evidence that does not support pyruvate kinase M2 (PKM2)-catalyzed reaction as a rate-limiting step in cancer cell glycolysis. *J. Biol. Chem.* **291**, 8987–8999
 43. Xie, J., Wu, H., Dai, C., Pan, Q., Ding, Z., Hu, D., Ji, B., Luo, Y., and Hu, X. (2014) Beyond Warburg effect—dual metabolic nature of cancer cells. *Scientific Rep.* **4**, 4927
 44. Gibon, Y., and Larher, F. (1997) Cycling assay for nicotinamide adenine dinucleotides: NaCl precipitation and ethanol solubilization of the reduced tetrazolium. *Anal. Biochem.* **251**, 153–157
 45. Ying, M., Guo, C., and Hu, X. (2019) The quantitative relationship between isotopic and net contributions of lactate and glucose to the TCA cycle. *J. Biol. Chem.* **294**, 9615–9630
 46. Zhang, W., Guo, C., Jiang, K., Ying, M., and Hu, X. (2017) Quantification of lactate from various metabolic pathways and quantification issues of lactate isotopologues and isotopomers. *Scientific Rep.* **7**, 8489
 47. Giachelli, C. M. (2003) Vascular calcification: *In vitro* evidence for the role of inorganic phosphate. *J. Am. Soc. Nephrol.* **14**, S300–S304
 48. Mendez, E. (2008) Biochemical thermodynamics under near physiological conditions. *Biochem. Mol. Biol. Educ.* **36**, 116–119
 49. Alberty, R. A. (2006) Biochemical thermodynamics: Applications of Mathematica. *Methods Biochem. Anal.* **48**, 1–458
 50. Li, X., Wu, F., Qi, F., and Beard, D. A. (2011) A database of thermodynamic properties of the reactions of glycolysis, the tricarboxylic acid cycle, and the pentose phosphate pathway. *Database (Oxford)* **2011**, bar005
 51. Keleti, T., Foldi, J., Erdei, S., and Tro, T. Q. (1972) Some thermodynamic data on D-glyceraldehyde-3-phosphate dehydrogenase action under optimal conditions. *Biochim. Biophys. Acta* **268**, 285–291
 52. Donnovan, L., Barclay, K., Otto, K., and Jespersen, N. (1975) Thermochimistry of reaction catalyzed by lactate-dehydrogenase. *Thermochim. Acta* **11**, 151–156
 53. Varga, A., Szabo, J., Flachner, B., Gugolya, Z., Vonderviszt, F., Zavodszky, P., and Vas, M. (2009) Thermodynamic analysis of substrate induced domain closure of 3-phosphoglycerate kinase. *Febs Lett.* **583**, 3660–3664
 54. Rekharsky, M. V., Egorov, A. M., Galchenko, G. L., and Berezin, I. V. (1981) Thermodynamics of redox reactions involving nicotinamide adenine-dinucleotide. *Thermochim. Acta* **46**, 89–101